Punching shear performance of reinforced concrete slab-to-steel column connections incorporating ECC and UHPECC

Engineering Structures 322 (2025) 119145

Contents lists available at ScienceDirect

Engineering Structures

journal homepage: www.elsevier.com/locate/engstruct

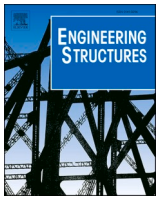

Punching shear performance of reinforced concrete slab-to-steel column connections incorporating ECC and UHPECC

Ahmed Hamoda [a], Aref A. Abadel [b], Mizan Ahmed [c], Vincent Wang [d], Zora Vrcelj [d], Qing Quan Liang [d,*,1]

[a] Department of Civil Engineering, Faculty of Engineering, Kafrelsheikh University, Kafrelsheikh, Egypt
[b] Department of Civil Engineering, College of Engineering, King Saud University, Riyadh 11421, Saudi Arabia
[c] Centre for Infrastructure Monitoring and Protection, School of Civil and Mechanical Engineering, Curtin University, Kent Street, Bentley, WA 6102, Australia
[d] College of Sport, Health, and Engineering, Victoria University, PO Box 14428, Melbourne, VIC 8001, Australia

ARTICLE INFO

Keywords:
Punching shear
High-performance concrete
Engineered cementitious composite
Nonlinear finite element modeling

ABSTRACT

Unlike the conventional reinforced concrete (RC) slab-column connection, the punching shear generated at the RC slab-to-steel column connection may lead to brittle punching shear failure due to the small area around the steel column. Moreover, the unexpected moments arising from eccentric loading can also lead to the failure of the slab in punching shear mode. This paper proposes employing high-performance concrete (HPC) to fill the critical punching shear zone to improve the punching shear resistance of RC slabs to steel column joints. Experiments on eight RC slabs to steel column connections are reported. The test parameters under investigation are the type of HPC used to fill the critical punching shear zone, the distance (S) of the HPC zone measured from the flanges of the steel column and loading condition (concentric and eccentric). The types of HPC include engineered cementitious composite (ECC) and ultra-high performance ECC (UHPECC). The experimental results show that the proposed techniques can significantly improve the cracking load, elastic stiffness, energy absorption capacity, ductility, failure modes, and ultimate load of the slab-to-column connections. The ultimate load of the tested connections is increased by as much as 33 %, and 28 % for the slabs subjected to concentric and eccentric loading, respectively. However, the ultimate load and energy absorption capacity of the slab with UHPECC having a S value of 1d, where d is the effective depth are lower than those of the control slab. Three-dimensional nonlinear finite element models are developed to simulate the performance of tested slab-to-column connections and validated by experimental results. The parametric study shows that the n (=S/d) value greater than 3.5 has insignificant effects on the ultimate punching shear capacity of the slab. It is demonstrated that the proposed formulas faithfully estimate the ultimate punching shear capacity of slab-to-column connections constructed with different HPCs under concentric and eccentric loadings.

1. Introduction

Steel–concrete composite systems have been vastly utilized in construction applications [1–3]. In reinforced concrete (RC) flat slabs, RC slab-steel-I-column composite connection is often adopted due to its simplicity and lower cost associated with the shortened construction time [4,5]. However, such a system suffers from excessive stresses arising from punching shear forces due to the smaller cross-sectional area of the steel I-column [6,7]. Punching shear is one of the common but undesirable failure modes in RC flat slabs which is a brittle type of failure [8]. The punching shear failure at the slab-to-steel column connection may result in the overloading of other zones and can cause the entire structure to collapse due to potential progressive collapse. Therefore, it is essential to strengthen the slab-to-steel-column connection not only to enhance the load-carrying capacity but also to allow the load re-distribution to occur in the vicinity of failure [9–11].

The performance of RC slab-steel-I-column composite connection has been extensively studied in recent years. The use of additional stirrups or drop panels has been extensively investigated in order to improve the punching shear performance of RC flat slabs. Zhou et al. [12] carried out

* Corresponding author.
E-mail address: Qing.Liang@vu.edu.au (Q.Q. Liang).
[1] https://orcid.org/0000-0003-0333-2265

https://doi.org/10.1016/j.engstruct.2024.119145
Received 3 April 2024; Received in revised form 23 September 2024; Accepted 14 October 2024
Available online 21 October 2024

Table 1
Details of the test specimens.

Group	Name	Loading case	Flexural Reinforcement (%)	Existence of post-casting zone	Distance from column (S)	Concrete type
G0	S-C	C	0.4 %	———	———	NC
	S-E	E		———	———	NC
G1	S-C	C	0.4 %	———	———	NC
	S-E	E		———	———	NC
	S-U-C−10	C		Exist	S=d (100 mm)	NC+UHPECC
	S-U-E − 10	E		Exist	S=d (100 mm)	NC+UHPECC
G2	S-C	C	0.4 %	———	———	NC
	S-E	E		———	———	NC
	S-H-C−15	C		Exist	S= 1.5d (150 mm)	NC+ECC
	S-H-E − 15	E		Exist	S= 1.5d (150 mm)	NC+ECC
G3	S-C	C	0.4 %	———	———	NC
	S-E	E		———	———	NC
	S-U-C−20	C		Exist	S= 2d (200 mm)	NC+UHPECC
	S-U-E − 20	E		Exist	S= 2d (200 mm)	NC+UHPECC

C=concentric; E = eccentric

experimental work on nine simply supported slab–column connections to examine punching shear performance. The effectiveness of a proposed slab–column connection embedded with a steel skeleton and the influence of reinforcement ratio and slab thickness were studied. The test results showed that the proposed slab–column connection improved the punching shear capacity of the slab-column connection and improved the failure modes. Such improvement can be achieved by using fibrous high-performance concrete such as ECC and UHPECC. Luu et al. [13] examined the effects of an innovative connection comprising bearing plate and vertical ribs on the punching shear performance and the deformation capacity of the unbounded-post tensioned (UPC) slab-concrete filled steel tube (CFST) column joints. The studied parameters emphasized that the proposed innovative connection system improved the ultimate capacity by 10 %, ultimate deformation by 39 %, and energy consumption by 25 % compared to the control slab–RC column connection. Rafiee et al. [14] investigated the performance of post-tensioned slab–steel column connections numerically subjected to inverted-cyclic punching force. Their results showed that the post-tensioned level, vertical shear force, and dimensions of steel plates significantly affected the seismic performance of slab–steel column connections. Ungermann et al. [15] studied the punching shear performance of column–thick RC slab connections. Four concentrically and fourteen eccentrically loaded slab–column connections were tested up to collapse. It was found that eccentric loading greatly affects the performance of slab-column connections.

Previous investigations have also recommended applying high-performance concrete (HPC) material as a practical solution for increasing slab-column connections' load-carrying capacity and ductility [16–18]. Some research has been conducted experimentally and numerically to assess the punching shear behavior of flat slabs made of HPC [19–22]. Wang et al. [19] examined the behavior of steel-concrete composite slabs constructed by UHPC subjected to concentric load. Cakmak et al. [21] evaluated the accuracy of various design methods for computing the punching shear capacity of UHPC flat plates. Zhou et al. [23] performed an experimental study to explore the post-cracking punching shear performance of concrete slabs partially reinforced with full-depth ultra-high performance concrete (UHPC). The test results showed that the failure mode of flat slabs can be changed from brittle punching to ductile one associated with the flexural modes. Fang et al. [24] investigated the shear performance of grouped rubber-sleeve studs embedded in UHPC beams for bridge applications. It was found that the composite system significantly improved the structural behavior of the beams. Fang et al. [25] examined the shear performance of single-embedded-nut-bolted shear connectors in steel-UHPC beams by performing push-out tests. It was reported that the performance of steel-UHPC beams was significantly affected by the diameter and grade of shear connectors, degree and sequence of pre-tension, concrete casting method, and connector type. Ramos et al. [26] studied the responses of slab-column connections with HPC subjected to reversed cyclic loading. Test results showed that the cyclic performance of slab-column connection with HPC significantly improved. Isufi et al. [27] also used HPC in the vicinity of slab-column connections subjected to concentric loading. It was found that the ultimate load of the slab with HPC was increased by up to 58 % compared to the control slab without HPC.

The use of ECC and the new kind of ultra-high-performance engineered cementitious composite (UHPECC) may improve the punching shear resistance of connections due to their high strain-hardening performance and higher tensile and compressive strengths. However, investigation has been minimal on the punching shear performance of RC slab–steel I-column connections subjected to concentric and eccentric loading. Therefore, this paper presents an experimental and numerical investigation into the punching shear behavior of RC slab-to-steel column connections incorporating post-cast UHPECC/ECC in critical punching shear zones. Nonlinear three-dimensional finite element models (FEMs) are also developed by employing Abaqus and validated by the experimental results. Formulas are proposed for calculating the punching shear capacities of the slab-to-steel column connections with HPC under concentric and eccentric loadings.

2. Experimental program

2.1. Details of test specimens

Eight RC slabs were grouped into four Groups, as shown in Table 1. All slabs had identical dimensions for both the slab and the steel-I column. The slab dimensions were 1000 × 1000 × 120 mm^3, with an effective depth (d) of 100 mm, while the standard I section with dimensions as shown in Fig. 1(a) was used as a steel I-column. The thickness of the slab was selected based on the previous study carried out by Hamoda and Hossain [8] to ensure that the punching shear failure mode was captured to avoid local failure. Extensive tests on slab-column connections with a thickness of 120 mm and below can be found in the literature [3]. The test parameters studied herein are: (1) the type of post-cast HPCs (i.e., UHPECC and ECC), (2) the distance (S) of the HPC zone on one side was measured from the flange of the steel I column (i.e., S=1d, 1.5d, and 2d; where d is the effective depth measured from the top surface to the flexural reinforcement) and (3) loading condition (i.e., concentric and eccentric). The Group G0 was set as the control group to assess the effect of concentric and eccentric punching shear force as illustrated in Fig. 1b and Fig. 1(c), respectively. The eccentric load was applied by attaching the steel I-beam to the steel

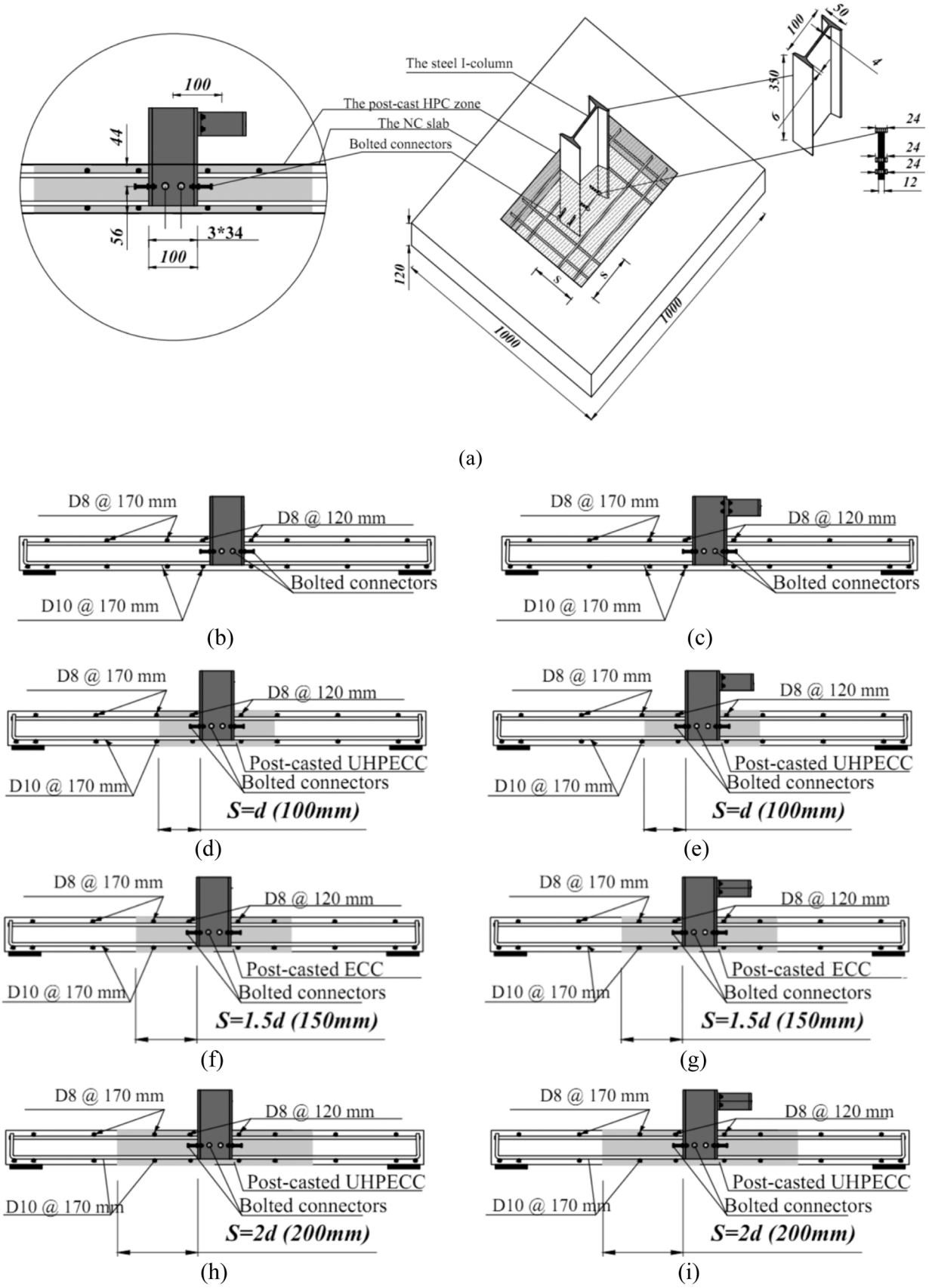

Fig. 1. Schematic details of the tested slabs with I column; (a) Three-dimension view of the variables (b) Slab S-C; (c) Slab S-E (d); Slab S-U-C-10; (e) Slab S-U-E-10; (f) Slab S-H-C-15; (g) Slab S-H-E-15; (h) Slab S-U-C-20; and (i) Slab S-U-E-20.

Table 2
Properties of polypropylene fiber.

Diameter (μm)	Length (mm)	Tensile strength (N/mm^2)	Young's modulus, (GPa)	Density (gm/cm^3)	Elongation (%)
39	10	950	44.5	0.97	20

I-column, giving an eccentricity of 100 mm as shown in Fig. 1(c). The slabs in G0 were entirely made of normal strength concrete (NC) and labeled as S-C and S-E subjected to concentric and eccentric loading, respectively. The slabs in Groups, G1, G2, and G3, had post-cast intermediate connections filled with UHPECC, ECC, and UHPECC, respectively, as described in Table 1 and Fig. 1(d to i). Table 1 shows that the G1 group comprised the slabs S-U-C-10 and S-U-E-10 loaded concentrically and eccentrically, as shown in Fig. 1(d and e), respectively, together with the two control slabs included for comparison purposes. Slabs S-U-C-10 and S-U-E-10 were constructed with NC; however, the zone around the steel column with a distance (S) of S=d (i.e., S=100 mm) measured from the outer flange of the I-column in one side was filled with UHPECC as shown in Fig. 1(d and e). Specimens in G2 were constructed identically to Group G0 except that the zones around the steel column in specimens (S-H-C-15 and S-H-E-15) were cast with ECC with S= 1.5d (i.e., S=150 mm) as detailed in Table 1 and shown in Fig. 1(f and g). In Group G3, UHPECC was utilized to fill the slab–steel column joints of specimens S-U-C-20 and S-U-E-20 with S= 2d

Table 3
Mix proportions of concrete and measured strengths.

Concrete	Cement (kg/m^3)	F.Agg (kg/m^3)	C.Agg. (kg/m^3)	F.A. (kg/m^3)	S.F	W/b	PP (kg/m^3) (%)	HRWR (kg/m^3)	f_c (N/mm^2)	f_t (N/mm^2)	Elastic modulus (N/mm^2)
NC	355	698	1143	—	—	0.42	—	—	32	2.56	19800 ± 0.02
UHPECC	800	500	—	750	150	0.27	19 (2 %)	40 (S.P)	129	11.85	48076 ± 0.02
ECC	558	436	—	665	—	0.23	20 (2 %)	15	52	4.43	26923 ± 0.03

Note: Cement grade 52.50 N/mm^2, F.Agg.: fine aggregate, C.Agg.: Coarse aggregate, F.A.: Fly ash, S.F.: silica fume, W/b: water to binder ratio (binder=Cement+F.A+S.F), PP: polypropylene fiber, HRWR: high range water reducer, S.P: superplasticizer.

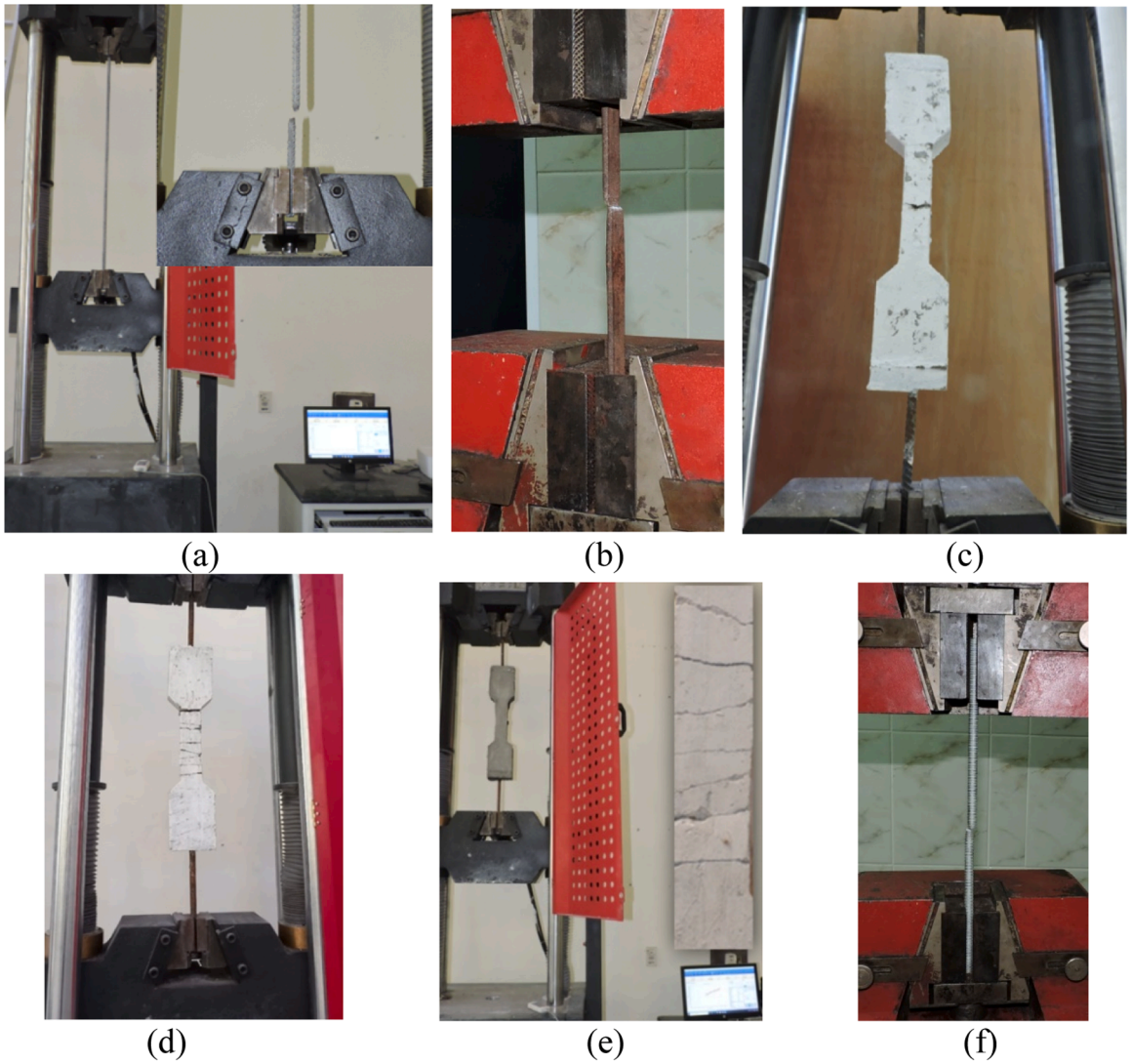

Fig. 2. Direct tensile tests; (a) Steel bars, (b) steel plate for I-column; (c) NC (d) ECC (e) UHPECC, (f) Sample of steel bolt.

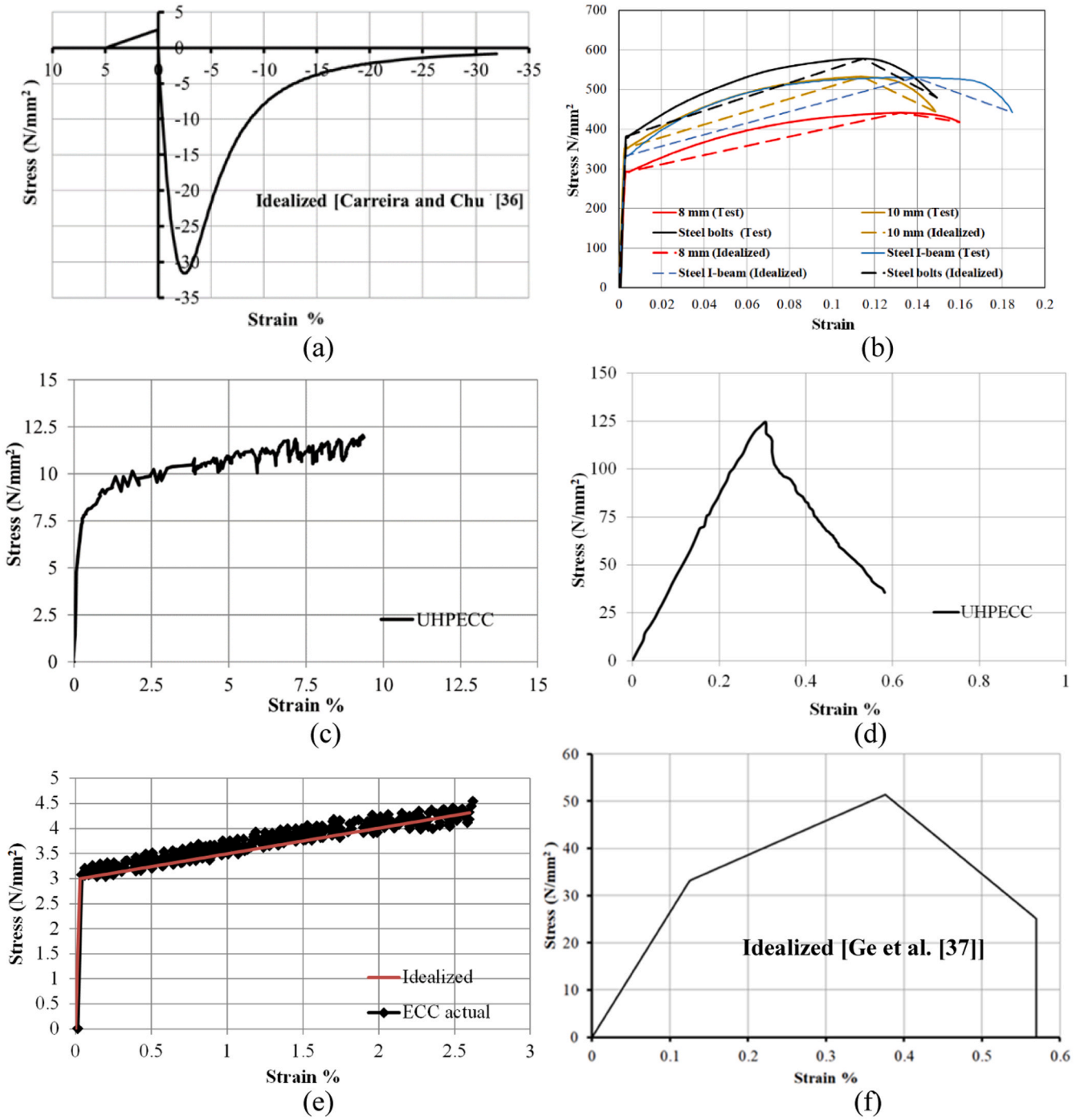

Fig. 3. Stress-strain relationships of (a) NC under compression and tension; (b) Steel bars; (c) UHPECC under tension; (d) UHPECC under compression; (e) ECC under tension; and (f) ECC under compression.

Table 4
Material properties of steel elements.

Steel element	Existence	yield stage		ultimate stage		E (GPa)	Poisson`s Ratio
		σ_y (MPa)	ε_y (%)	σ_u (MPa)	ε_u (%)		
8 mm	Compressive steel	291	0.154	442	13.11	189	0.30
10 mm	Flexural steel	349	0.176	529	12.23	197	0.30
Steel plate	I-Column	365	0.181	532	14.01	202	0.30
Steel bolts	Shear connector	382	0.189	578	11.45	203	0.30

σ: Stress; ε: Strain; E: Modulus of elasticity.

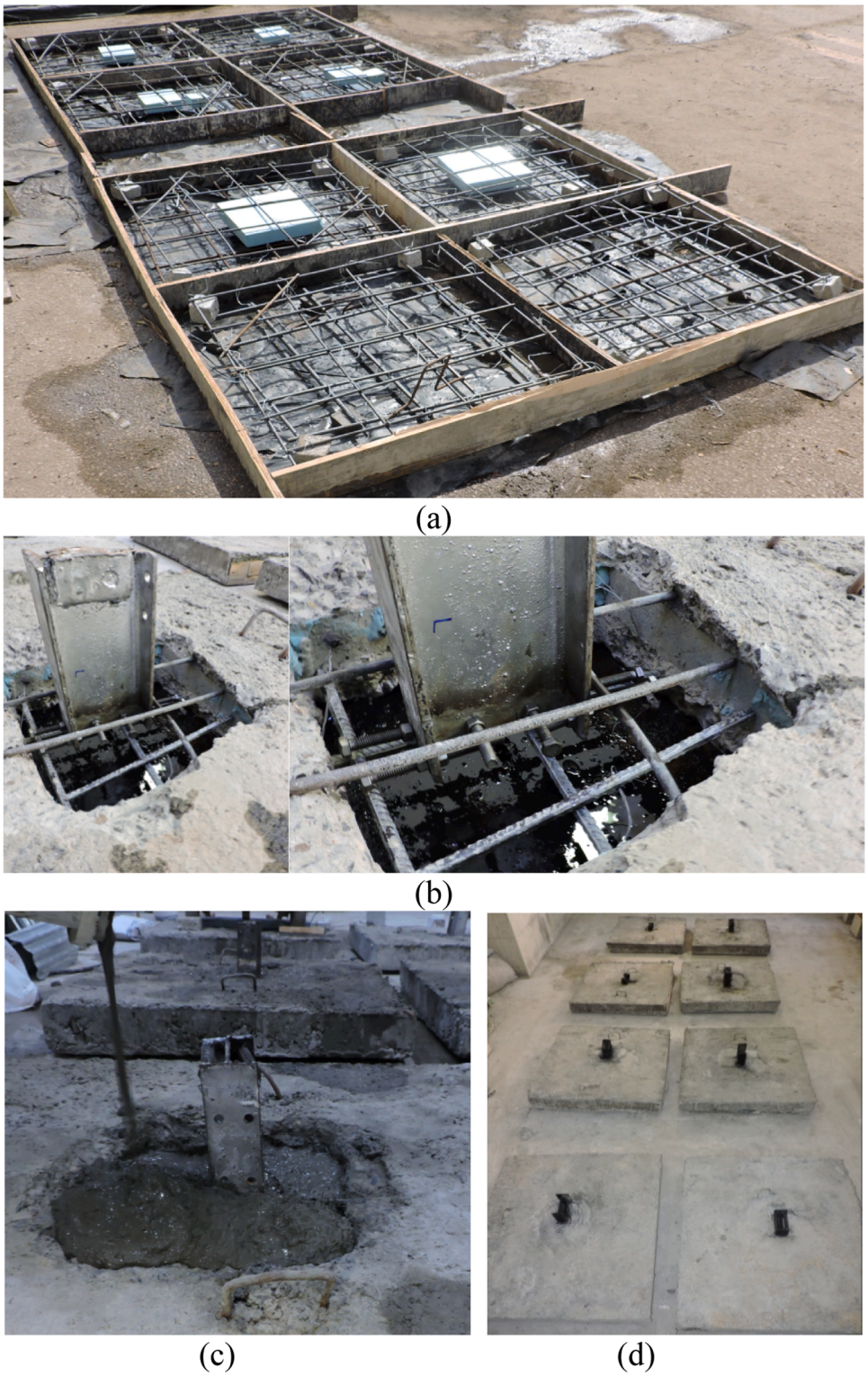

Fig. 4. Casting and preparation of slabs: (a) Wooden formwork and foam location; (b) Steel I-column-slab connection; (c) UHPECC; (d) All slabs before testing.

(i.e., S=200 mm) as shown in Fig. 1(h and i), respectively, and Table 1.

2.2. Properties of steel and concrete

Two types of HPCs, namely ECC and UHPECC were employed at the punching shear zone to improve the structural performance of NC slab-steel-column joints. The ECC was characterized by its higher strain hardening and better ductility, while the UHPECC had a performance similar to the ECC besides having higher strength. In this study, UHPECC was made of polypropylene (PP) fiber similar to existing studies [28,29]. The properties of PP fiber are provided in Table 2. The flowability of UHPECC and ECC with PP fiber was 185 and 160 mm, respectively. The conventional NC was used to pre-cast all slabs and the two control slabs. The mix proportions for each type are tabulated in Table 3. The UHPECC mix was similar to that employed previously by Zeng et al. [29]. The compression tests of the concrete materials were carried out according

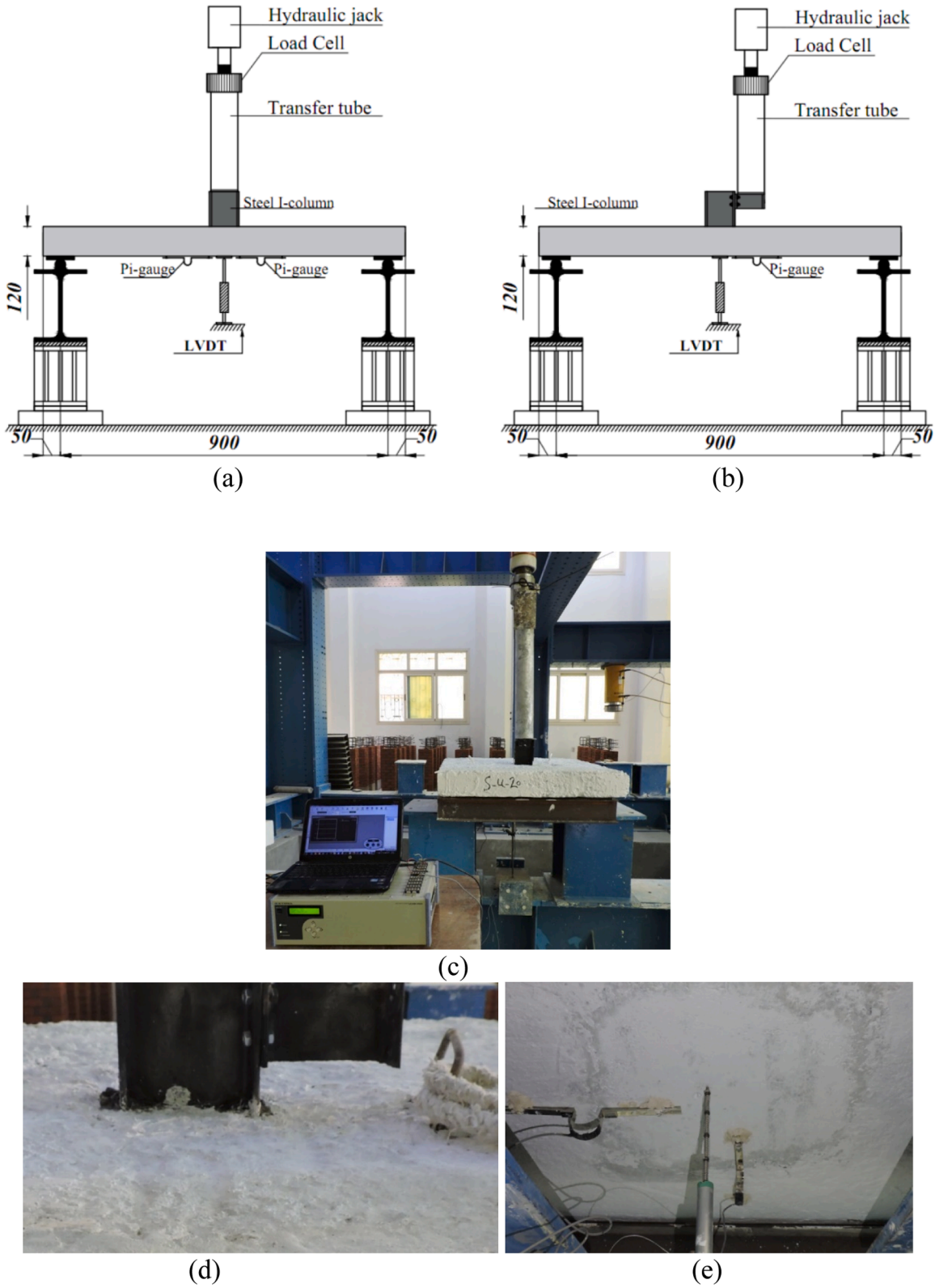

Fig. 5. Test set-up and instrumentation: (a) Schematic detail and dimensions for concentric loading (units: mm); (b) Schematic detail and dimensions for eccentric loading (units: mm); (c) experimental setup; (d) case of eccentric loading; (e) arrangement of sensors.

to ASTM C39/C39M [30]. The compressive strength (f_c') shown in Table 3 was measured from three concrete cylinder tests with a dimension of 150 × 300 mm recommended by ACI 318–19 [31]. The elastic modulus of concrete was obtained directly from the testing machine that calculated the elastic modulus of concrete using ASTM C469/C469M [32] as specified by the manufacturer. The average elastic modulus for each type of concrete is shown in Table 3. The elastic modulus of UHPECC was calculated as 48076 MPa. A similar value was reported by Yu et al. [33] earlier. For ECC, the calculated elastic modulus of 26923 MPa was consistent with the test observation

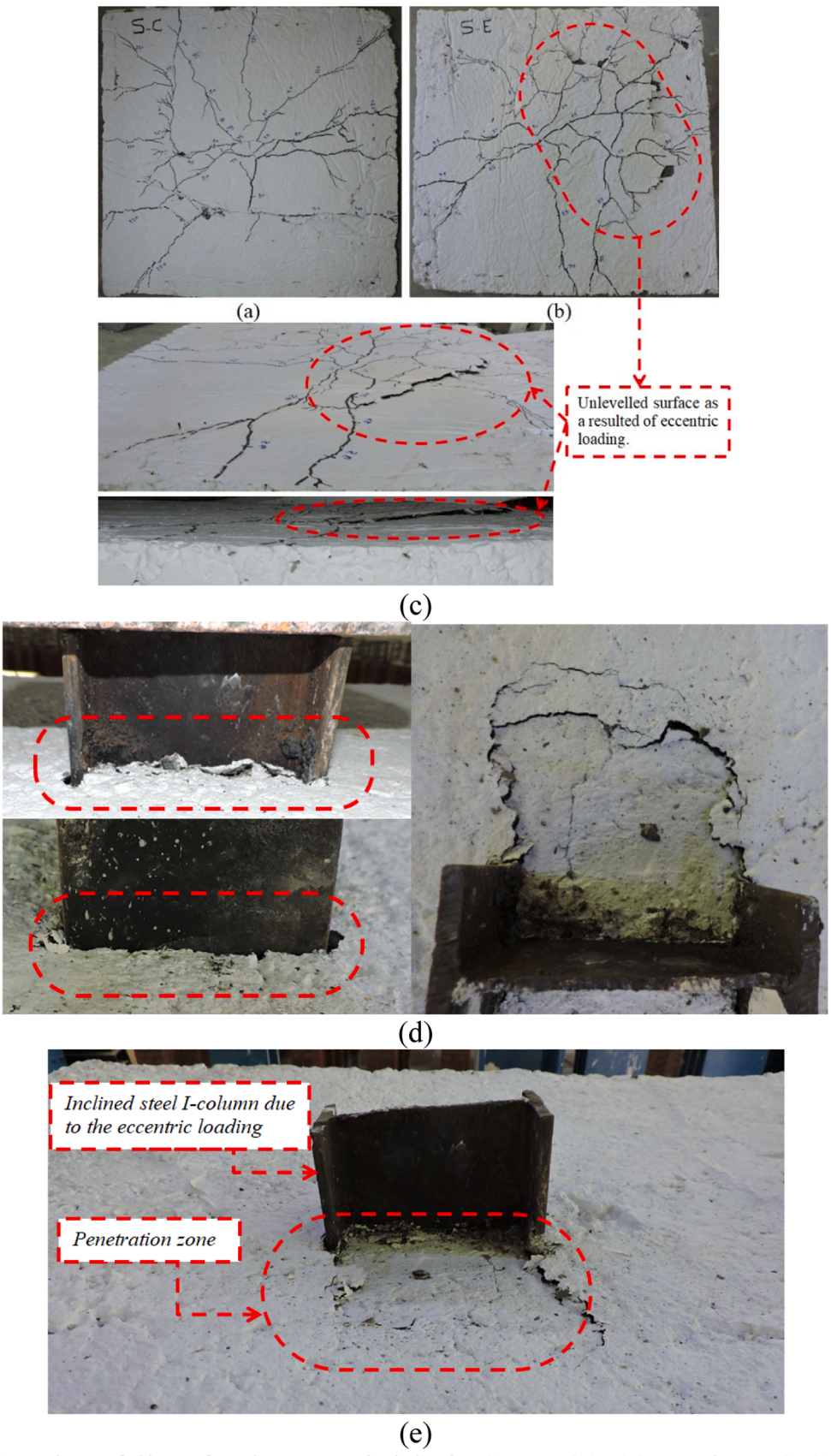

Fig. 6. Punching shear failure for the control slabs in Group G0: (a) specimen S-C; (b) specimen S-E; (c) Bottom and side view of specimen S-E; (d) Penetration of the steel I-column for S-C; (e) Penetration of the steel I-column for S-E.

reported by Mao et al. [34]. Mao et al. [34] found that the elastic modulus of ECC with various aspect ratios of fibers was within the range of 22000 MPa to 28000 MPa. However, the elastic modulus of normal strength concrete was 19800 MPa which is lower than that reported in the literature. This may be due to the fact that a smaller amount of fine aggregate was used to cast the concrete, which reduced its elastic stiffness. Direct tensile tests were conducted for NC, ECC, and UHPECC, as shown in Fig. 2 according to ASTM C1583 [35]. The uniaxial stress-strain responses of concrete are given in Fig. 3. The compressive stress-strain curves of NC and ECC were calibrated using the suggestion given by Carrier and Chu. [36] and Ge et al. [37], respectively.

Uniaxial tensile tests of steel elements were conducted according to A370–10 [38] as shown in Fig. 2. The 8-mm diameter steel bars used as compressive reinforcement had a yield and tensile strength of 291 and 442 MPa, respectively. The 10-mm diameter of deformed steel bars used as flexural reinforcement had a yield and tensile strength of 349 and 529 MPa, respectively. The yield and tensile strengths of the steel I-column were 365 and 532 MPa, respectively. Axial tensile testing of steel bolts was conducted as shown in Fig. 2(f). The yield and ultimate stresses were measured as 382 and 578 MPa, respectively. Table 4 summarizes the material properties of the tested steel elements. The actual and idealized stress-strain curves were captured and employed for the numerical simulation, as shown in Fig. 3.

2.3. Preparation of the slabs

All slabs with normal concrete were cast using wooden formworks, as shown in Fig. 4(a). Plastic foam was positioned at the mid-slab where the punching area was supposed to be post-casted with UHPECC or ECC. After one day, the NC slabs were de-molded and, for 28 days, cured in a

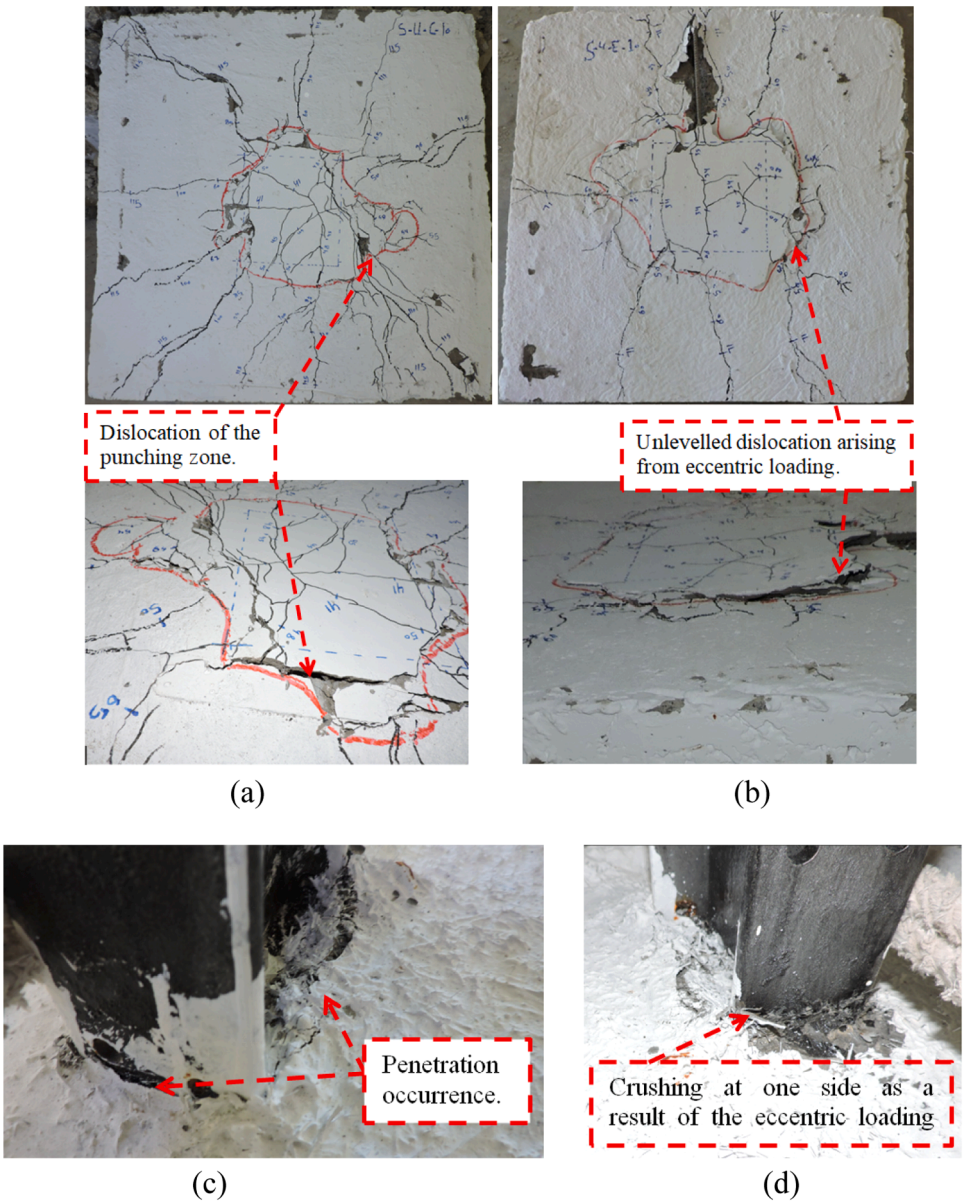

Fig. 7. Punching shear failure for NC- UHPECC composite slabs in group G1: (a) specimen S-U-C-10; (b) specimen S-U-E-10; (c) top surface of specimen S-U-C-10; and (d) top surface of specimen S-U-E-10.

wet environment and then allowed for air drying. Then, the plastic foam was cleaned, and the steel I-columns with designed demountable bolted connectors were embedded as columns into the slab, as shown in Fig. 4 (b). UHPECC (for G1 and G3) and ECC (for G2) were used to fill the punching shear zones, as can be seen in Fig. 4(c). An adequate bond between the NC and HPC was achieved by the friction between the concrete and reinforcement bars. All slabs before testing are shown in Fig. 4(d).

2.4. Test set-up and instrumentation

Fig. 5 illustrates the testing setup of the specimens. All slabs were rested on steel I-beams with welded bars at the top flange of the I-beam simulating pinned supports as presented in Fig. 5(a and b). Since the aim of this study was to determine the punching-shear performance of the slab-column connection, the test setup was accommodated to capture the punching failure similar to the one tested by Mansour et al. [39]. The deflection at the mid-zone of the bottom surface was measured using a Linear Variable Displacement Transducer (LVDT), as shown in Fig. 5(e). PI-gauges sensors were located near the interface line between the punching shear zone and the NC slab to record the cracking, as shown in Fig. 5(e). For each tested slab, a strain gauge was mounted on a flexural steel rebar to measure the steel strain and capture the yield load. A hydraulic machine with a capacity of 3000 kN was utilized to apply the load of the tested slabs with an increment rate of 2 kN/min. The eccentric load was applied by attaching the steel I-beam with the steel I-column, giving an eccentricity of 100 mm as shown in Fig. 5(b and d). A digital data logger was used to collect results from all sensors. Each slab was incrementally subjected to the applied load prior to collapse. The generated cracks were highlighted as appearing during the test until all slabs failed.

3. Test results and discussion

3.1. Deformed shape and failure mode

All slabs were subjected to concentric or eccentric punching force from initial stages up to collapse. The failure modes of all slabs are shown in Figs. 6–9. The results obtained from the tests are provided in Table 5 in which the cracking loads (P_{cr}) and their corresponding deflection (Δ_{cr}), and the ultimate load (P_u) and its corresponding deflection (Δ_u) were recorded.

The two control slabs (i.e., S-C and S-E) in G0 were loaded to failure, and the corresponding results were employed for comparison. The failure of both the concentrically and eccentrically loaded slabs is shown in Fig. 6(a and b), respectively. For both S-C and S-E, the first visible hair

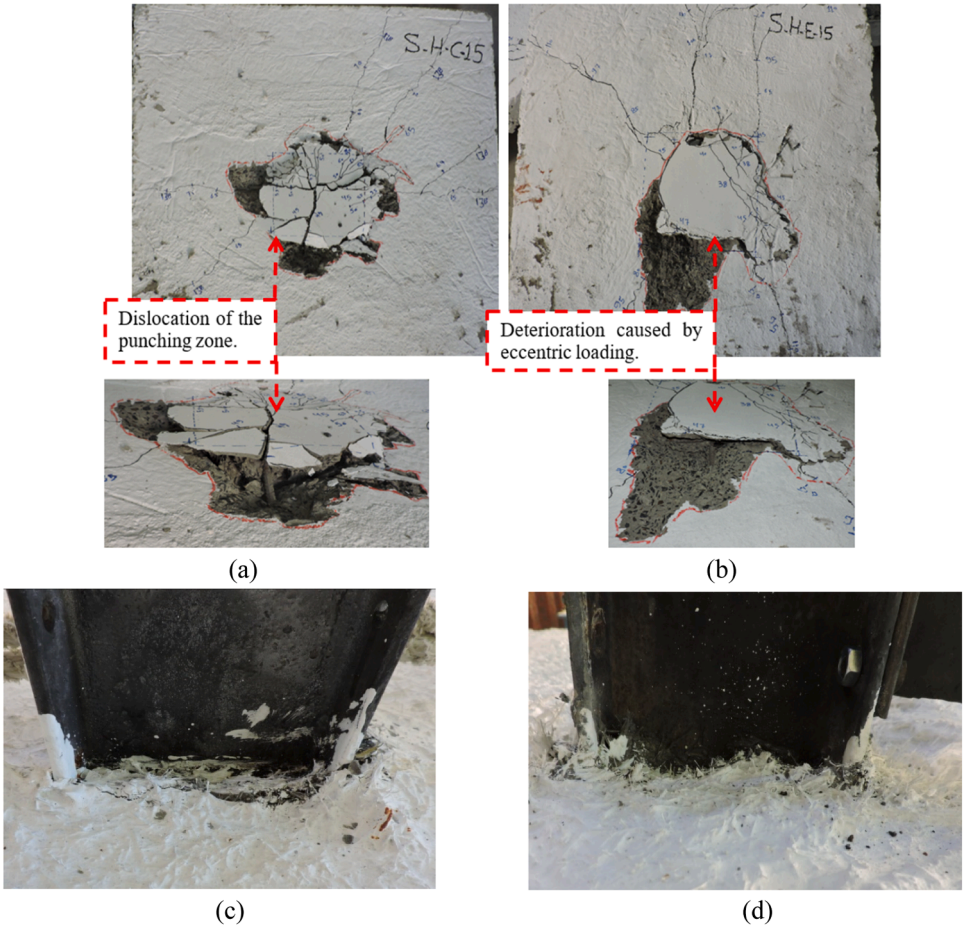

Fig. 8. Punching shear failure for NC-ECC composite slabs in group G2: (a) specimen S-H-C-15; (b) specimen S-H-E-15; (c) top surface for specimen S-H-C-15; and (d) top surface for specimen S-H-E-15.

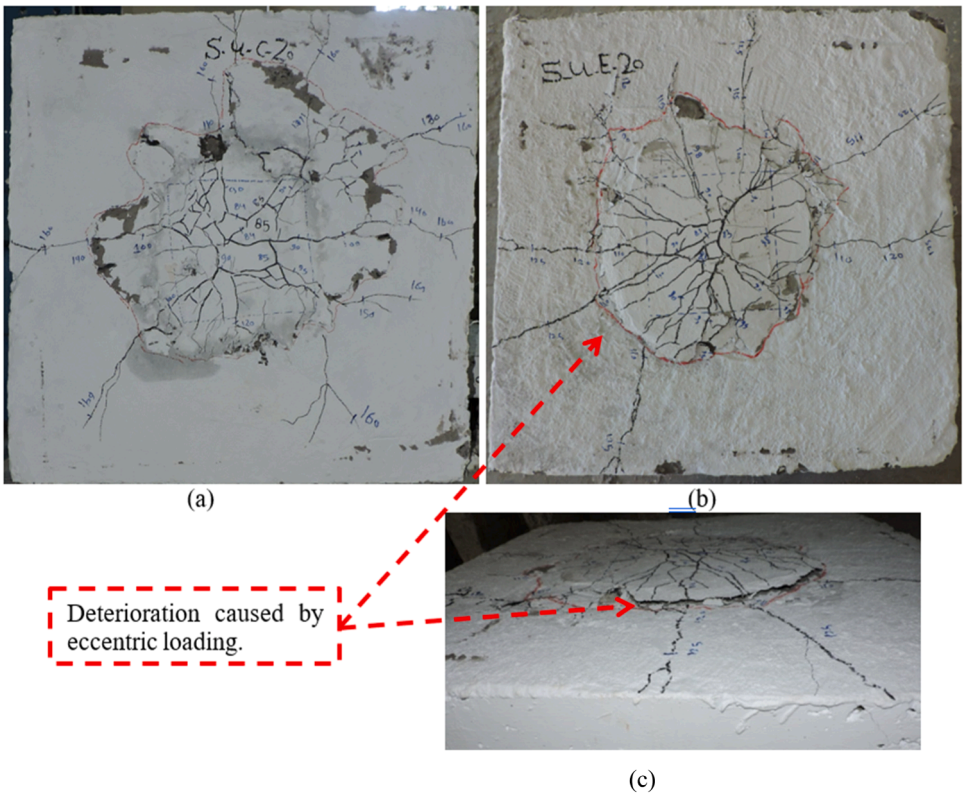

Fig. 9. Punching shear failure for NC-UHPECC composite slabs in group G3: (a) specimen S-U-C-20; (b) specimen S-U-E-20.

Table 5
Summary of the test results.

Group	Name	Cracking Stage				Ultimate Stage			Elastic stiffness (K)		Absorbed energy (AE)	
		P_{cr} (kN)	P_{crS}/P_{crS0}	w_{cr} (mm)	Δ_{cr} (mm)	P_u (kN)	P_{uS}/P_{uS0}	Δ_{Pu} (mm)	K	K_S/K_{S0}	AE	AE_S/AE_{S0}
G0	S-C	75	1.00	0.18	18.72	120	1.00	28.68	4.01	1.00	1842	1.00
	S-E	65	1.00	0.24	16.02	98	1.00	26.25	4.06	1.00	1300	1.00
G1	S-U-C−10	41	0.55	0.28	8.03	115	0.96	21.37	5.10	1.27	1471	0.80
	S-U-E − 10	34	0.52	0.48	6.29	71	0.72	14.79	5.41	1.33	841	0.65
G2	S-H-C−15	45	0.60	0.22	6.16	138	1.15	27.49	7.30	1.82	3101	1.73
	S-H-E − 15	38	0.58	0.44	7.34	110	1.12	23.38	5.17	1.28	2315	1.78
G3	S-U-C−20	84	1.12	0.16	11.38	160	1.33	37.07	7.38	1.84	5876	3.19
	S-U-E − 20	83	1.28	0.20	14.41	125	1.28	26.34	5.76	1.42	1828	1.41

Notes:- P_y and Δ_y are defined as yield load and corresponding deflection, P_{cr} and Δ_{cr} are defined as cracking load and corresponding deflection, w_{cr} is defined as crack width measured at P_{cr}, P_u and Δ_u are defined as ultimate load and corresponding deflection.

crack appeared at the bottom surface close to the mid-zone at a load of about 75 kN and 65 kN (about 63 % and 66 % of P_u), respectively, as shown in Fig. 6. It can be seen from Table 5 that the width of the first crack in both S-C and S-E was about 0.18 mm and 0.24 mm, respectively. Then, cracks at the bottom zone spread towards the outer supports; however, some cracks extended diagonally at the corners. Such diagonal cracks were caused by the two-way action due to the square rectangularity, as previously reported [8]. When further loads were applied, the crack width increased with a remarkable appearance for eccentrically loaded slab S-E close to the quarter span because of eccentricity. Just before failure, the cracks increased, extending to the outer edges and intensively to the corners. A sudden brittle punching shear failure was recorded just at the ultimate load, which was about 120 kN and 98 kN for S-C and S-E, respectively. At the top surface of either of the two slabs in G0, the column seemed to be separated, generating a semi-rectangular form at the top surface penetrating the slab with complete dislocation of the punching cone as shown in Fig. 6(d and e).

The two specimens, i.e. S-U-C-10 and S-U-E-10, were tested to study the effect of post-cast UHPECC with S= 100 mm from the I-column's face to resist the punching loading. The crack pattern of the slabs S-U-C-10 and S-U-E-10 are shown in Fig. 7(a and b), respectively. At initial loads, the first cracking load of S-U-C-10 and S-U-E-10 was recorded to be about 41 kN and 34 kN (about 35 % and 47 % of P_u), with a crack width of about 0.28 mm and 0.48 mm, respectively. The lower P_{cr} value with a larger crack width, compared to the control slabs, may be due to the slab's discontinuity and a smaller post-cast zone. The appearance of the first crack for group G1 was recorded close to the interface surface at the bottom. As seen in Fig. 7(a and b), the surface of the shear punching failure was similar to conic shape which usually has an inclination of much less than 45°, thus resulting in a larger crack width and a smaller cracking load. With further increase in the loading, some cracks extended diagonally from the mid-slab zone towards the four corners, as shown in Fig. 7(a) for slab S-U-C-10 with the concentric condition. On the other hand, the opening of the cracks for the eccentric loading case seemed to be wider with each given load increment, as shown in Fig. 7

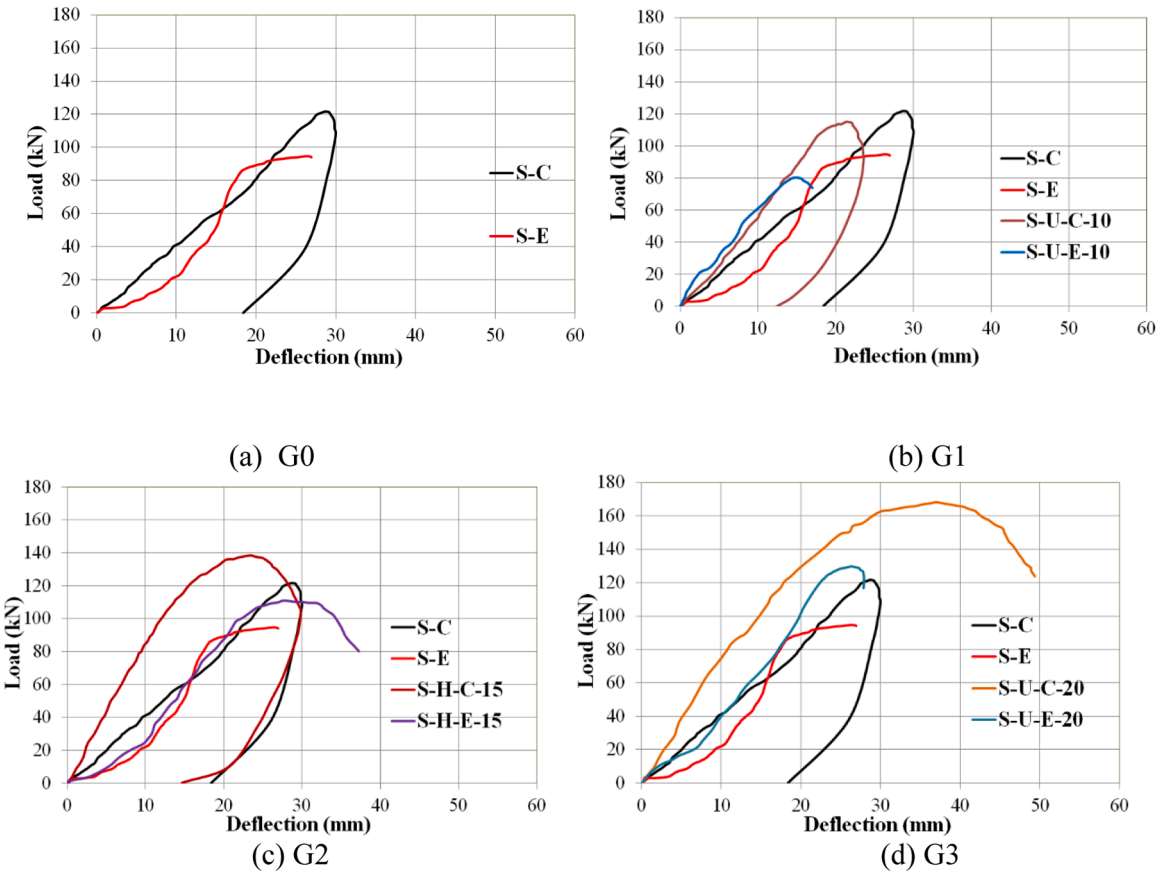

Fig. 10. Load-midspan deflection responses of tested slabs.

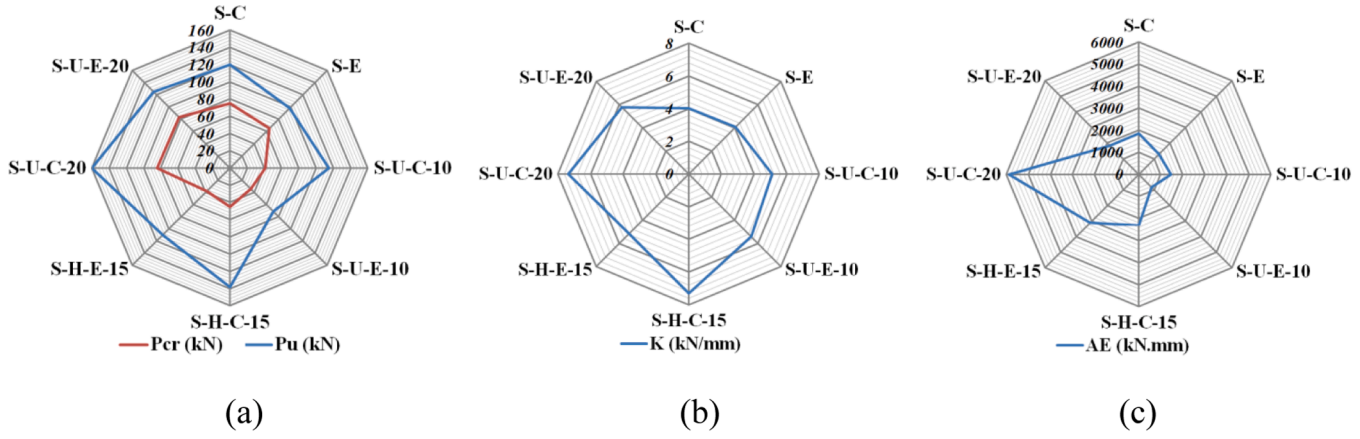

Fig. 11. Comparison of (a) loads; (b) elastic stiffness; and (c) absorbed energy of tested slabs.

(b) for slab S-U-E-10. Just before failure, the cracks enlarged with wider widths and grew intensively towards the outer edges. Punching shear failure occurred suddenly with a brittle appearance at P_u= 115 kN and 71 kN for the slabs S-U-C-10 and S-U-E-10, respectively. In the I-column-slab connection, as shown in Fig. 7(c and d), the column penetrated the slab's top surface with remarkable dislocation present in the central region of the slab, manifesting the punching shear failure.

Specimens in G2 (S-H-C-15 and S-H-E-15) were constructed with ECC with S= 150 mm. The first hairline crack was detected close to the interface surface at the bottom at 45 kN and 38 kN for the slabs S-H-C-15 and S-H-E-15 (about 32 % and 33 % of P_u). Table 5 shows that the initial cracks had widths of about 0.22 mm and 0.44 mm, respectively, for the slabs S-H-C-15 and S-H-E-15. A few cracks were detected at the mid-zone of the bottom surface with each load increment. Ductile punching shear failure was experienced, followed by steel buckling, as shown in Fig. 8. The peaked loads of slabs S-H-C-15 and S-H-E-15 were 138 kN and 110 kN, respectively.

The UHPECC was employed in Group G3 to fill the punching shear zone of the NC slab–steel I-column connection with S= 200 mm for S-U-C-20 and S-U-E-20 subjected to concentric and eccentric punching loading, respectively. Table 5 illustrates that the first cracking load values were about 84 kN and 83 kN for the slabs S-U-C-20 and S-U-E-20, respectively, which were higher than those of the control slabs by about 12 % and 20 %, respectively. The close-range P_{cr} values for both

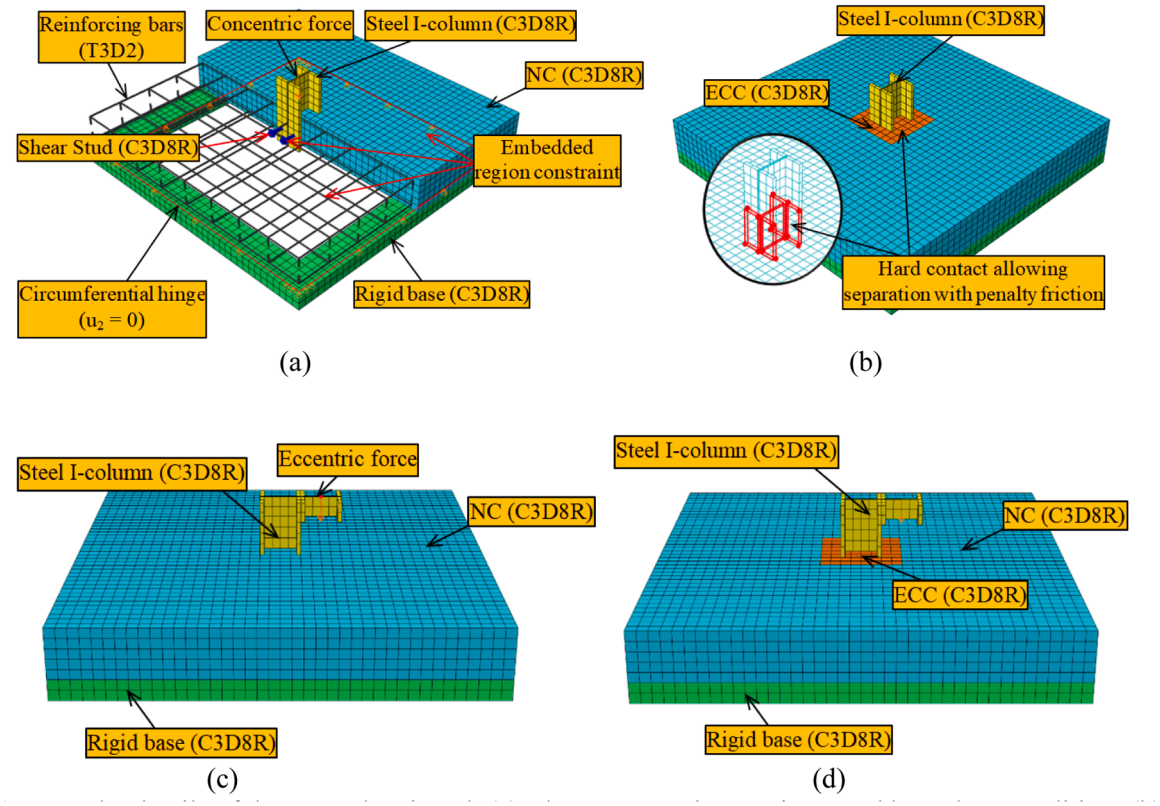

Fig. 12. The details of the FEM developed: (a) Element type, interactions, and boundary condition; (b) Interaction of the post-casted UHPECC or ECC zone; (c) Eccentric loading; (d) Eccentric loading of the slab with post-casted UHPECC or ECC.

Table 6
Comparison of the cracking and ultimate loads of the tested slabs.

Specimens	Cracking load			Ultimate load				
	$P_{cr.exp}$ (kN)	$P_{cr.FE}$ (kN)	$\frac{P_{cr.FE}}{P_{cr.exp}}$	$P_{u.exp}$ (kN)	$P_{u.FE}$ (kN)	$\frac{P_{u.FE}}{P_{u.exp}}$	$P_{up.cal}$ (kN)	$\frac{P_{up.cal}}{P_{up.exp}}$
S-C	75	72	0.96	120	126	1.05	-	-
S-E	65	60	0.93	98	100	1.02	-	-
S-U-C−10	41	39	0.95	115	108	0.94	113	0.98
S-U-E − 10	34	33	0.97	71	79	1.11	76	1.07
S-H-C−15	45	43	0.96	138	134	0.97	135	0.98
S-H-E − 15	38	37	0.97	110	112	1.02	109	0.99
S-U-C−20	84	81	0.96	160	163	1.02	162	1.01
S-U-E − 20	83	79	0.95	125	130	1.04	127	1.01
Average			0.95			1.02		1.01
Standard deviation (SD)			0.02			0.05		0.03
Coefficient of Variance (CoV)			0.02			0.05		0.03

eccentric and concentric punching force revealed that the slab–steel I-column connection filled with UHPECC with S= 200 mm could compensate for the excessive stresses arising from the eccentricity. Moreover, the better performance can also be evidenced by the first cracking formed within the UHPECC zone, avoiding the interface surface, with cracking widths of 0.16 mm and 0.20 mm for S-U-C-20 and S-U-E-20, respectively. With further loads and just before failure, several random cracks grew from the mid-zone of the bottom surface, as shown in Fig. 9 with the full absence of any significant cracks happening at the interface. Unlike the brittle one, soft failure punching mode with dislocation of the mid-zone induced by excessive punching shear force with an ultimate load of 160 kN and 125 kN for both the slabs S-U-C-20 and S-U-E-20, respectively (enhancing the ultimate loads by about 33 % and 28 % compared to the two control slabs).

3.2. Loads

Table 5 presents both the cracking and ultimate load values of all specimens. As shown in Table 5 and Fig. 10, within the same group, the slabs subjected to eccentric load had lower cracking and ultimate loads than those subjected to concentric load. However, the cracking load of S-U-E-20 subjected to eccentric punching force was found to be very close to that of S-U-C-20, which was loaded concentrically, as seen in Table 5. Nonetheless, the ultimate load of S-U-C-20 was higher than that of S-U-E-20. The comparison of the cracking and ultimate loads of the tested slabs is shown in Fig. 11 (a). As seen in Table 5, utilizing HPC in the critical punching shear zone of the RC slab–column connection reduces the deflection at the cracking stage compared to the control slab subjected to either concentric or eccentric loading. The improvement in the

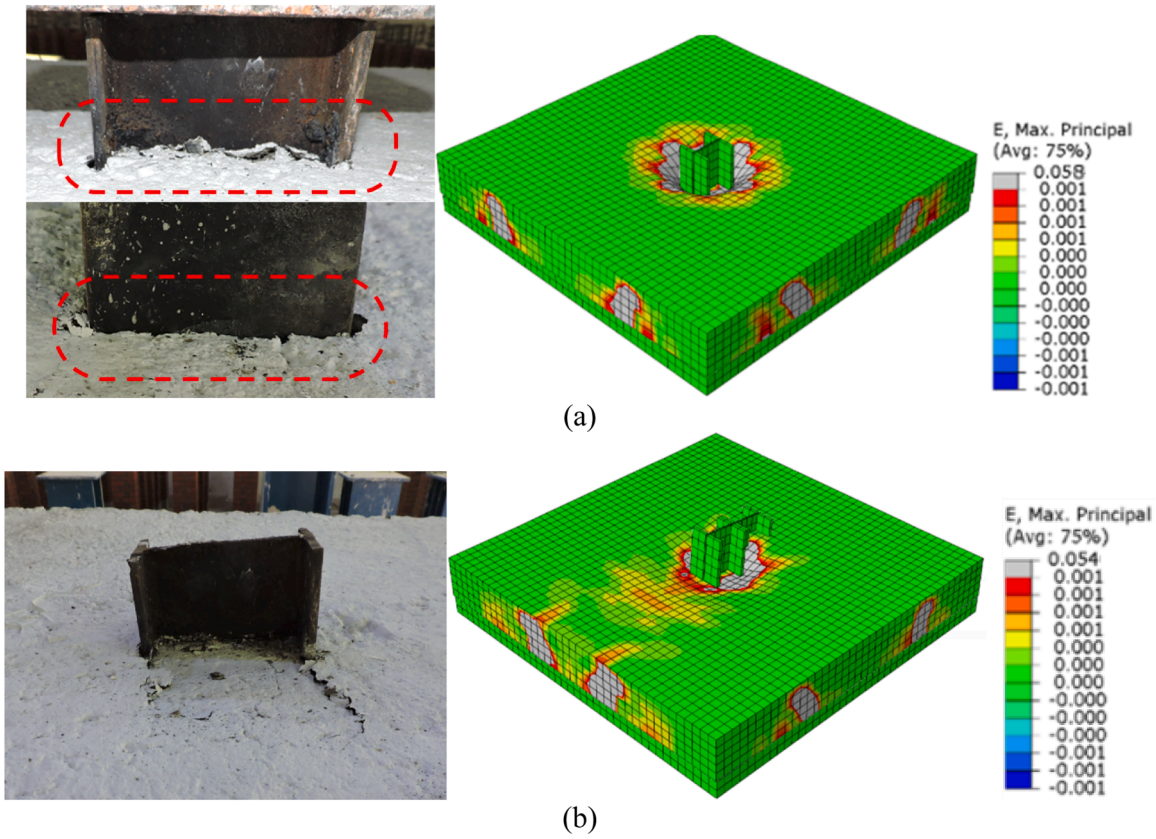

Fig. 13. Comparison of the punching failure mode of the group G0 (a) specimen S-C0; and (b) specimen S-E0.

cracking load for the slabs with S= 2d subjected to concentric or eccentric loading (S-U-C-20 and S-U-E-20) was calculated as 12 % and 27 % compared to the control slabs (S-C and S-E), respectively.

Slabs in Groups G2 and G3 improved in the ultimate load compared to control slabs. For slabs in Group G2, the ultimate loads of slabs S-H-C-15 and S-H-E-15 are 15 % and 12 % higher than those of S-C and S-E, respectively. Similarly, for slabs in Groups G3, the ultimate loads of slabs S-H-C-20 and S-H-E-20 are 33 % and 28 % higher than those of S-C and S-E, respectively.

3.3. Load-deflection response

The recorded load-deflection relationships of tested composite slabs are shown in Fig. 10. Table 5 shows the deflection values associated with both the cracking and ultimate loads (Δ_{cr}) and (Δ_u), respectively. Generally, all the slabs loaded concentrically exhibited linear performance followed by with or without hardening features up to the peaked zone. The control slab S-C and S-U-C-10 presented linear behavior up to the peak load, as shown in Fig. 10 (b). The significant hardening was noticeable for slabs with S= 1.5d and 2d as manifested in slabs S-H-C-15 and S-U-C-20 as shown in Fig. 10 (c and d). However, S-U-C-20 showed the largest deflection compared to other slabs, as shown in Fig. 10 (d). This is due to the larger UHPECC post-cast zone of the slab in group G3. The large cast zone improved the stress distribution, thus improving the ductility of the specimens. The eccentrically loaded slabs had lower load-carrying capacity than the ones loaded concentrically, as seen in Fig. 10 (a), as expected due to the eccentricity. Test results revealed that for the same type of concrete (group G1 and G3), the use of a 2d post-cast UHPECC zone presented larger cracking and ultimate load under eccentric loading. This is due to the improvement of the stress distribution, which improved the cracking of the specimens and led to the improvement of the loading capacity.

3.4. Elastic stiffness and absorbed energy

All tested specimens' elastic stiffness and absorbed energy were analyzed to investigate their elasticity and ductility. The elastic stiffness index (K) was measured as the slope of the linear part of the load-deflection response for the tested slab and is presented in Table 5 and Fig. 11 (b). The absorbed energy (AE) was expressed as the total area under the load-deflection relationship up to the ultimate load stage [40], as provided in Table 5 and Fig. 11 (c).

The presence of post-cast UHPECC and ECC resulted in a higher elastic stiffness of all slabs. The increase in the elastic stiffness for a concentrically loaded slab was calculated as 27 %, 82 %, and 84 %, for slabs in Groups G1, G2, and G3, respectively. The specimen with the larger cast zone exhibited a higher stiffness value which can be attributed to the improvement of the stress distribution. For the eccentrically loaded slabs, the increase in the elastic stiffness was calculated as 33 %, 28 %, and 42 % for the slab in Groups G1, G2, and G3, respectively. The better elastic performance can be attributed to the superior resistance of both UHPECC and ECC. Like the specimens under concentric loading, for the same type of concrete (group G1 and G3), the larger cast zone exhibited a higher stiffness value.

The tested parameters confirmed that the absorbed energy significantly depends on the clear distance of the post-cast concrete zone around the steel I-beam. Table 5 illustrates that those specimens with ECC and UHPECC generally exhibited higher absorbed energy for a S value greater than 1d than the control specimens under concentric or eccentric loading. For example, the AE value of specimens S= 1.5d filled

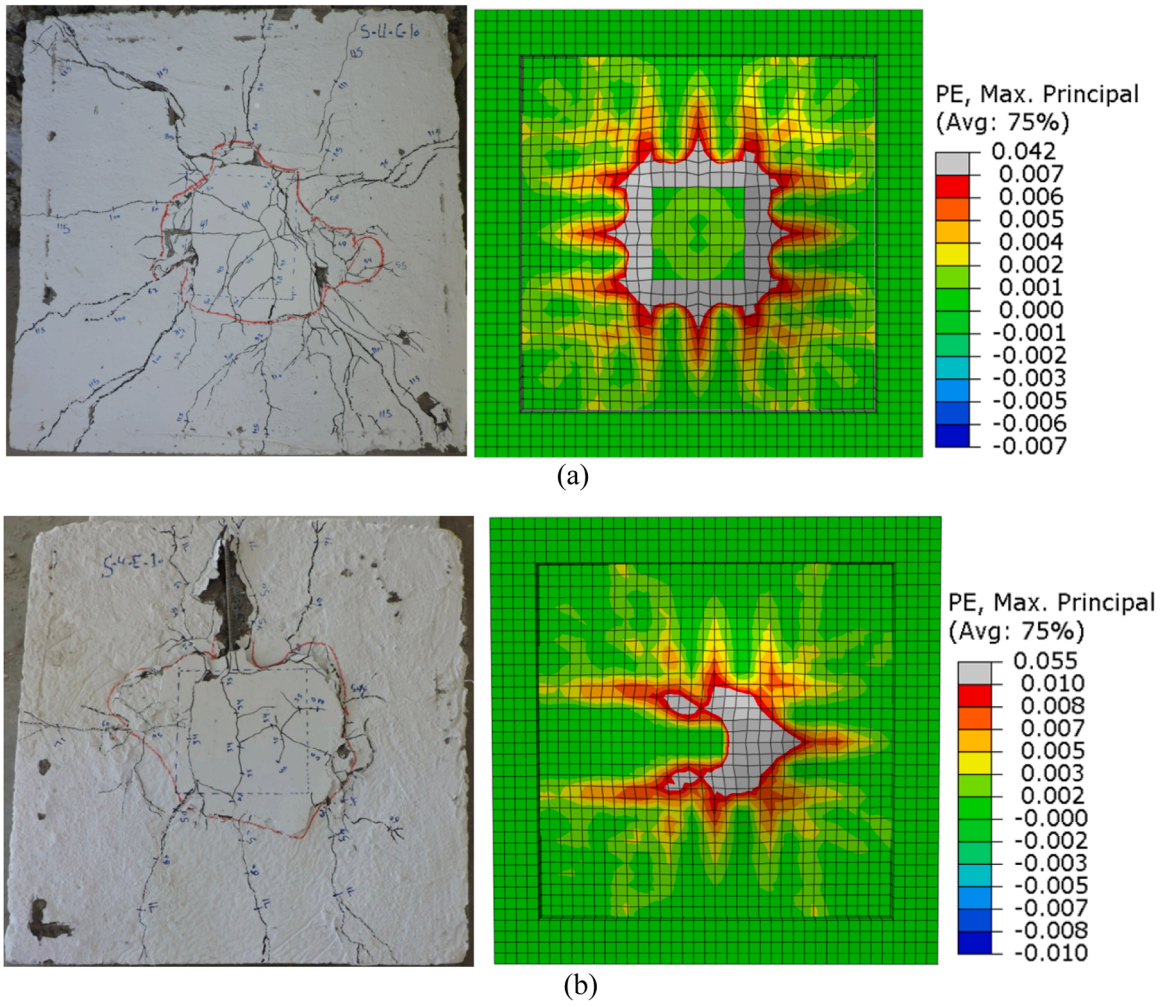

Fig. 14. Comparison of the punching failure mode of the group G1 (a) specimen S-U-C-10; and (b) specimen S-U-E-10.

with ECC increased by about 73 % to 78 % for concentric and eccentric conditions, as shown in Table 5. However, for specimens in Group G1, the absorbed energy of S-U-C-10 and S-U-E-10 was 20 % and 35 % less than that of the control specimens S-C and S-E, respectively. The more significant increase in the absorbed energy was recorded for the specimen with UHPECC having S= 2d under concentric loading where an improvement of the absorbed energy of 219 % was obtained compared to the control one. This may be due to the improvement of the stress distribution which improved the ultimate load and the ductility of the specimen.

4. Finite element modeling

The RC slabs tested herein were numerically modeled using the nonlinear three-dimensional software Abaqus [41]. Abaqus explicit method has been used for solving. The accuracy of the constructed models was established by comparing the predicted results against those obtained experimentally.

4.1. Constitutive materials laws

The Concrete Damage Plasticity (CDP) model was used to simulate the characteristics of concrete material. This model utilizes isotropic damage linearity, tension plasticity, and isotropic compression to better model the plastic performance in both compression and tension as reported previously [42–45]. Based on the CDP model, the softening of concrete was modeled using two damage variables namely d_c and d_t [46]. The values of these parameters ranged from 0 to 1, where zero represents undamaged materials and 1 represents total loss of strength. These parameters were calculated using Eqs. 1- 2 [46]:

$$\sigma_c = (1 - d_c)E_0(\varepsilon_c - \varepsilon_c^{pl}) \quad (1)$$

$$\sigma_t = (1 - d_t)E_0(\varepsilon_t - \varepsilon_t^{pl}) \quad (2)$$

where σ_c, and ε_c are the concrete compressive stress and the strain corresponding to σ_c; σ_t, and ε_t are the concrete tensile stress and the strain corresponding to σ_t; E_0, ε_c^{pl}, and ε_t^{pl} are the modulus of elasticity and the equivalent compression and tension plastic strains, respectively.

The idealized stress-strain curves of NC, ECC, and UHPECC, as shown in Fig. 3, which were calibrated with relevant experimental results, were implemented in the current modeling. To reduce the computational cost, the experimental stress-strain relationship of steel parts was idealized, as depicted in Fig. 3(b). To calibrate the FEMs, abundant attempts were executed to ascertain appropriate values for the sensitive parameters of the CDP model. The sensitive factors defining the CDP model are the ratio of biaxial to uniaxial compressive stresses (f_{bo}/ f_{co}), dilation angle (ψ), the ratio of the steady tensile stress to the compressive meridian (K_c), the eccentricity (e), and viscosity variable (μ). Such CDP parameters were considered in NC: 1.16, 29°, 0.67, 0.10, and 0.00, respectively

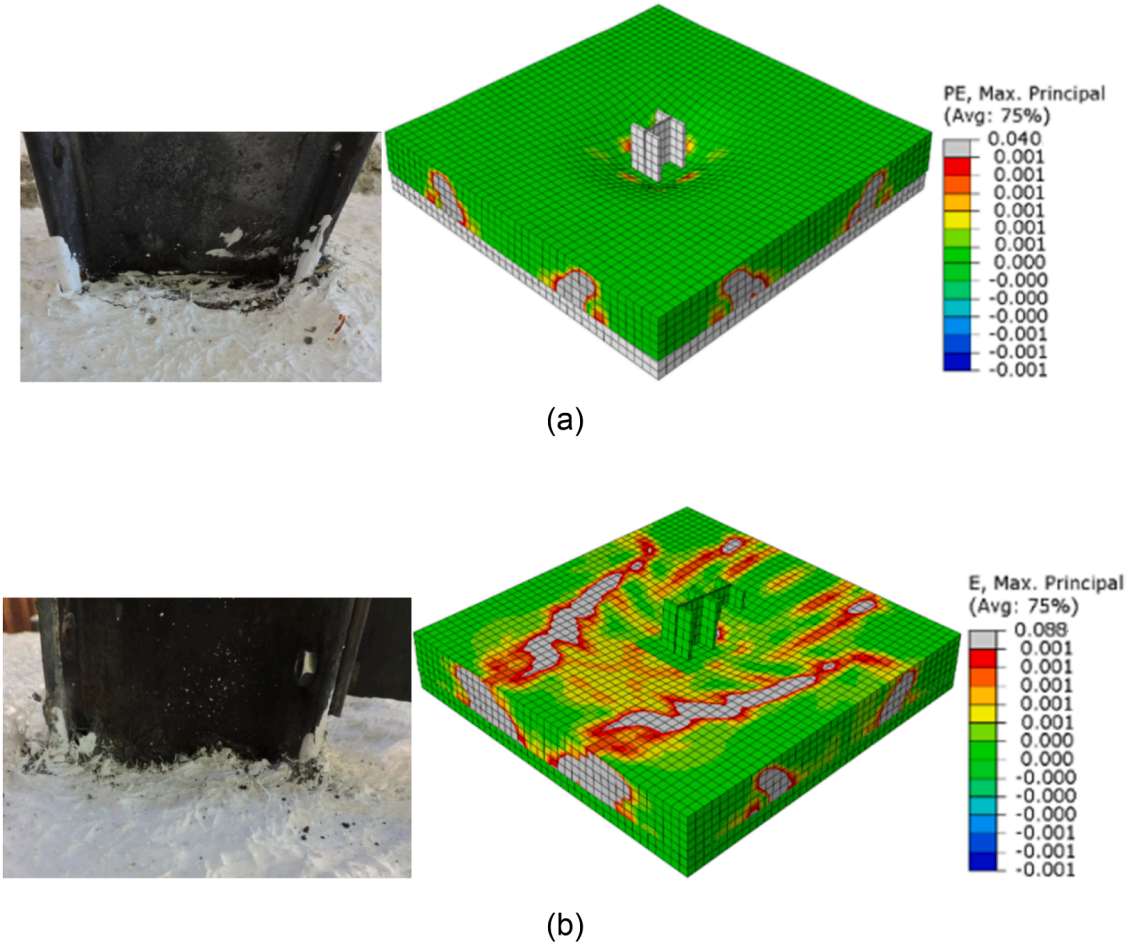

Fig. 15. Comparison of punching failure mode of NC-ECC composite slabs in group G2 (a) specimen S-H-C-15; and (b) specimen S-H-E-15.

[47,48]. In both ECC and UHPECC, the same parameters as NC were used except for dilation angle and viscosity, which were 34° and 0.000001 for ECC and 37° and 0.000001 for UHPECC, respectively, which were very close to those established in previous studies [47–52].

4.2. Model set-up

As shown in Fig. 12, an eight-node element (C3D8R) was used to model all concrete parts, the steel I column, and the supports. The steel bars were simulated by employing two-node and linear truss element (T3D2), as shown in Fig. 12. Steel bars interacted with the whole concrete slab through the embedded element system, available in ABAQUS, assuming a full bond between them. In this strategy, the concrete slab was selected as the host zone, while the steel bar was treated as the embedded one. Surface-to-surface contact was used to model the interface between NC and the post-cast UHPECC/ECC, with a friction coefficient of 0.6 employed in the tangential directions [43]. Such interaction was simulated by selecting the four inner side surfaces of the NC slab as the master zone, while the four outer surfaces of post-cast HPCs (ECC or UHPECC) were slave ones. All models were rested on four thick steel plates with more considerable stiffness set as supporting plates along the outer edges, simulating pinned boundary conditions as shown in Fig. 12. Finally, based on executed models with different mesh sizes, economic models were selected with a mesh size of 24 mm.

4.3. Verifications of FEM

This section outlines the accuracy of the numerical models by comparing them to the experimental results. Table 6 compares the cracking and ultimate loads predicted by the FEMs with the corresponding test results. The average ratio between the numerical and experimental results was about 0.95 and 1.02 for the cracking and ultimate stages, respectively, with a corresponding coefficient of variation (CoV) of 0.02 and 0.05. It should be noted that the cracking load was taken when the strain exceeded the tensile strain of concrete. Figs. 13–16 compare the failure modes of tested specimens. Similar to those that failed experimentally, the numerical models predicted the initiation of the cracking stresses to be just at the mid-zone of the bottom surface where the punching stresses critically existed. Under concentric loading, with the increased load, stresses started to extend towards the outer sides like those recorded experimentally as shown in Fig. 14 (a) and Fig. 16 (a). Under the eccentric loading condition, the predicted failure modes of specimens with UHPECC and the experimental modes are compared in Fig. 14 (b) and Fig. 16 (b). The numerical model produced critical punching stresses visualized asymmetrically at the bottom surface attributing the eccentric punching shear loading captured experimentally. It has been found that the developed models are capable of accurately simulating the experimental punching failure modes of tested specimens under concentric and eccentric loads. Fig. 17 presents

the comparisons of the load-deflection responses of all the tested slabs. It can be observed that the developed FEMs show good agreement with the experimental results.

5. Parametric study

The validated numerical model was used to conduct a parametric study on the effect of different n (=S/d) values on the ultimate punching shear capacity (P_{up}). The n values of 1, 1.5, 2, 2.5, 3, 3.5, and 4 were considered in the analyses. The punching shear zones constructed with either ECC or UHPECC under eccentric and concentric loads were investigated. The dimensions and the reinforcement arrangements for the analyzed slab-column connections were the same as the ones tested in this study. The distance (S) varied from 1d to 4d, where d is the effective depth. The effects of different effective depths up to 100 mm were also analyzed during the sensitivity analysis. Fig. 18 illustrates the effects of n values on the ultimate punching shear capacity of the slab-column connection for the effective depth of 100 mm. It is seen from Fig. 18 that increasing the n value increases the punching shear capacity (P_{up}) of the slab-to-steel column connections. However, when n value is greater than 3.5, increasing n value has insignificant effects on the increase in the punching shear capacity of the connections regardless of the loading conditions. Therefore, it is recommended that the post-cast zone be constructed with UHPECC or ECC with an n value not exceeding 3.5. The load-deflection responses of slabs with UHPECC or ECC subjected to concentric and eccentric loadings for various S values are shown in Fig. 19. It appears that increasing S values increases the initial stiffness and final deflection of the slabs.

Based on the parametric study, the following formulas are proposed for calculating the ultimate punching shear capacity (P_{up}) of slab-column connections incorporating UHPECC or ECC subjected to concentric and eccentric loadings within the range of 1d≤S≤ 4d.

For slab-to-steel column connections under concentric loading,

$$P_{up} = \left(-0.18n^2 + 1.24n + 0.55\right)A_p \quad \text{for UHPECC} \tag{3}$$

$$P_{up} = \left(-0.17n^2 + 1.19n + 0.52\right)A_p \quad \text{for ECC} \tag{4}$$

For slab-to-steel column connections under eccentric loading,

$$P_{up} = \left(-0.2n^2 + 1.32n - 0.03\right)A_p \quad \text{for UHPECC} \tag{5}$$

$$P_{up} = \left(-0.18n^2 + 1.2n + 0.17\right)A_p \quad \text{for ECC} \tag{6}$$

where $A_p$is the punching shear area (in mm^2) and calculated as the product of the shear perimeter and the effective depth of the slab; P_{up}in Eqs. (3–6) is in Newton. The accuracy of the proposed design equations

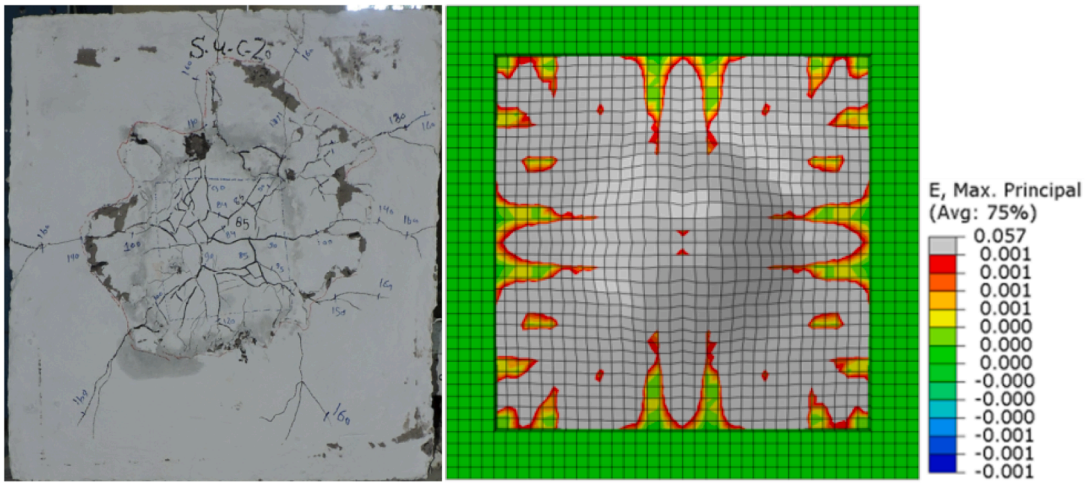

(a)

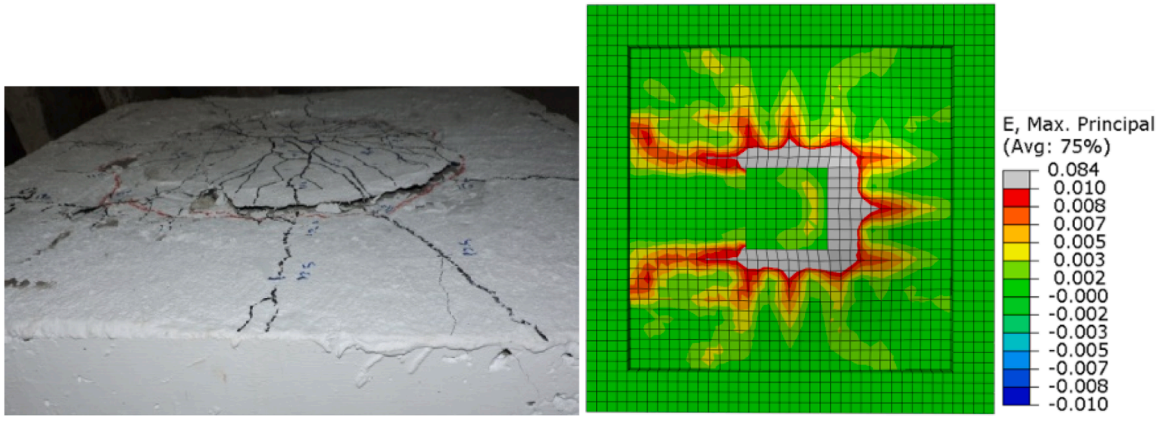

(b)

Fig. 16. Comparison of flexural- punching failure for NC-UHPECC composite slabs in group G3: (a) Model S-U-C-20; and (b) specimen S-U-E-20.

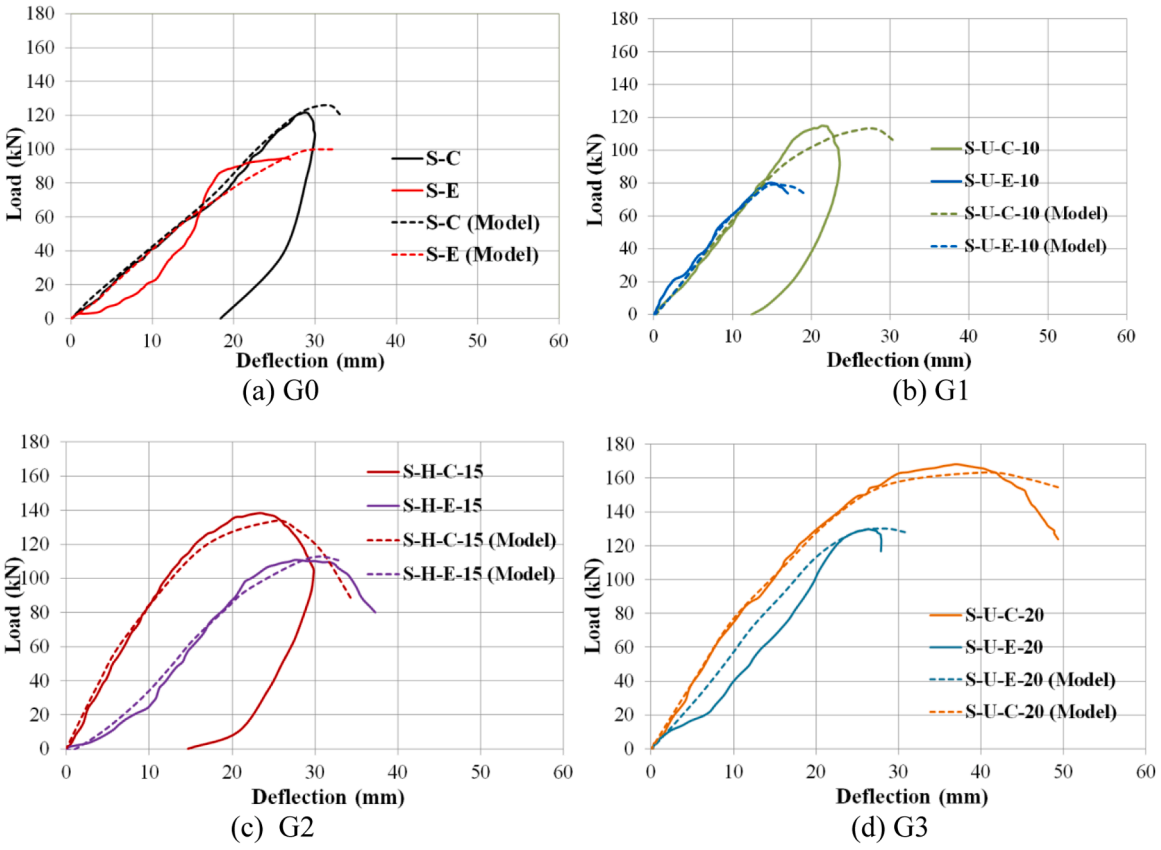

Fig. 17. Comparison of the experimental and numerical load-mid-span deflection responses of tested slabs.

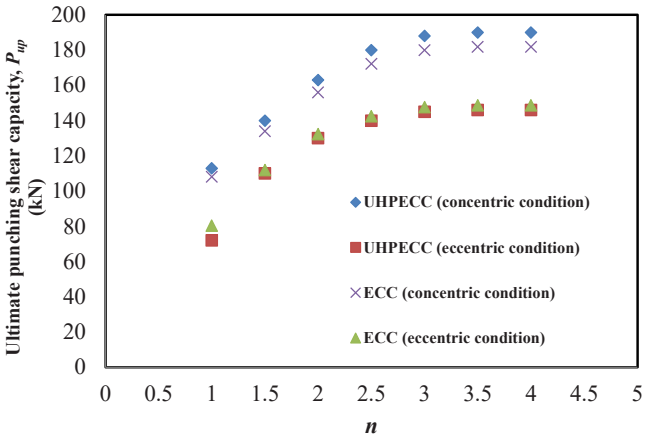

Fig. 18. Effect of different n values on the ultimate punching shear capacity of slab-column connections for the effective depth of 100 mm.

is validated by comparing the calculated ultimate punching shear capacities of slab-column connections test results and finite element solutions. It can be seen from Table 6 that the proposed formulas can accurately predict the ultimate punching shear capacities of slab-column connections with UHPECC or ECC subjected to concentric and eccentric loadings. The mean value of the prediction-to-experimental ultimate punching shear capacity is 1.01, with a standard deviation of 0.03. It can be seen from Table 7 that the agreement between the calculations and the FE predictions is good. The mean value of the prediction-to-FE ultimate punching shear capacity is 1.00 for slab-column connections under concentric and eccentric loading with a standard deviation of 0.03 and 0.02, respectively.

6. Conclusions

This paper has presented experimental and numerical investigations into the punching shear performance of RC flat slabs supported over steel I-section columns subjected to concentric and eccentric loading incorporating ECC and UHPECC. The punching shear zones in slabs were post-cast with ECC and UHPECC with clear distances of 1, 1.5, and 2 times the effective depth of the slab. Numerical models were also developed using Abaqus and their predictions were compared against the test results to validate their accuracy. The following conclusions are drawn from this study:

1. The slabs with UHPECC improved the ultimate load by 15 % and 33 % for the S values of 1.5d and 2d, respectively, when compared with the control slab subjected to the concentric loading. For the eccentric loading, the improvement was 12 % and 27 %, respectively. However, for S=d, the slab's ultimate load was less than the ultimate load of the control slabs that were subjected to either concentric or eccentric loading.
2. The only improvement in the cracking load was observed for the slabs with S= 2d subjected to either concentric or eccentric loading. The improvement in the cracking load for the slabs with S= 2d subjected to concentric or eccentric loading (S-U-C-20 and S-U-E-20) was 12 % and 27 % compared to the master slabs (S-C and S-E).
3. The elastic stiffness of all the tested slabs with ECC and UHPECC was significantly higher than that of the control slabs. The general trend

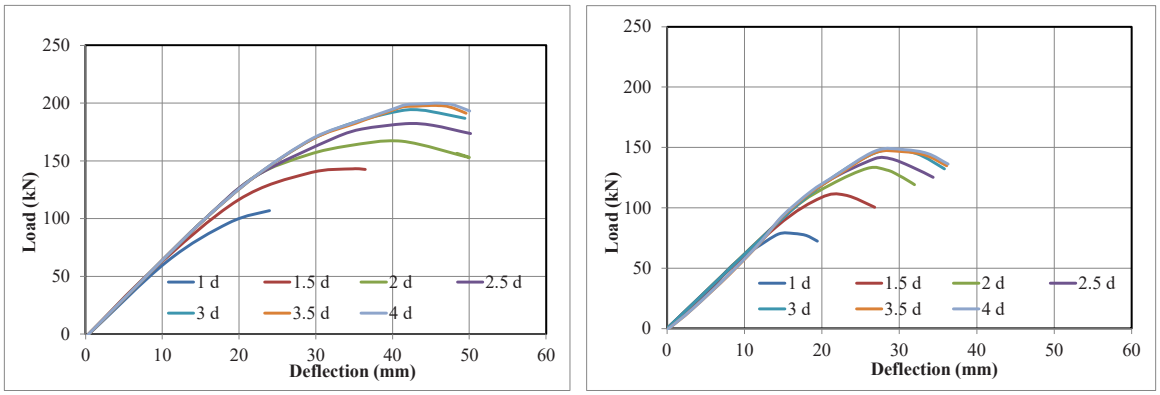

Fig. 19. Load-deflection responses of slab-to-column connections.

Table 7
Comparison of calculated ultimate punching shear capacities with FE results.

Type of concrete	n	Connections under concentric loading			Connections under eccentric loading		
		$P_{up.FE}$ (kN)	$P_{up.cal}$ (kN)	$\frac{P_{up.cal}}{P_{up.FE}}$	$P_{up.FE}$ (kN)	$P_{up.cal}$ (kN)	$\frac{P_{up.cal}}{P_{up.FE}}$
UHPECC	1.0	113	113	1.00	108	108	1.00
	1.5	140	140	1.00	134	135	1.00
	2.0	163	162	0.99	156	155	1.00
	2.5	180	177	0.98	172	170	0.99
	3.0	188	186	0.99	180	179	1.00
	3.5	190	188	0.99	182	182	1.00
	4.0	190	184	0.97	182	179	0.99
ECC	1.0	72	76	1.06	80	83	1.04
	1.5	110	105	0.95	112	110	0.98
	2.0	130	127	0.97	132	130	0.98
	2.5	140	141	1.01	143	143	1.00
	3.0	145	149	1.03	148	151	1.02
	3.5	146	150	1.03	149	152	1.02
	4.0	146	144	0.98	149	146	0.98
Mean				1.00			1.00
Standard deviation (SD)				0.03			0.02
Coefficient of Variance (CoV)				0.03			0.02

was that the higher the S value, the higher the elastic stiffness. The elastic stiffness of the slabs with the S values of 1.5d (S-U-C-15) and 2d (S-U-C-20) subjected to concentric loading was 82 % and 84 % higher than that of the control slab (S-C).

4. The energy absorption capacity of the slabs with S values of 1.5d and 2d showed remarkable improvement compared to the control slab. The slab with S= 2d (S-U-C-20) exhibited an improvement of 218 % in the energy absorption capacity compared to the control slab (S-C).
5. The predictions by the developed FEMs are in good agreement with the relevant experimental results, in particular, the ratio of the numerical to experimental results being 0.95 and 1.02 for the cracking and ultimate stages, respectively.
6. It is recommended to use a post-cast punching zone filled with UHPECC or ECC with n (=S/d) value not exceeding 3.5. The proposed formulas provide accurate predictions of slab-to-steel columns connections.

CRediT authorship contribution statement

Qing Quan Liang: Writing – review & editing, Supervision. **Zora Vrcelj:** Writing – review & editing, Visualization. **Vincent Wang:** Writing – review & editing, Visualization. **Mizan Ahmed:** Writing – original draft, Visualization, Formal analysis. **Aref A. Abadel:** Writing – original draft, Validation, Software, Project administration, Methodology, Investigation, Formal analysis, Data curation, Conceptualization. **Ahmed Hamoda:** Writing – original draft, Validation, Software, Methodology, Investigation, Formal analysis, Data curation, Conceptualization.

Declaration of Competing Interest

The authors declare that they have no known competing financial interests or personal relationships that could have appeared to influence the work reported in this paper.

Acknowledgment

The tests reported in this paper were carried out in the structural concrete laboratory at Kafrelsheikh University. The research funds provided by the Researchers Supporting Project number (RSP2024R343) from King Saud University, Riyadh, Saudi Arabia are acknowledged.

Data availability

Data will be made available on request.

References

[1] Yu JL, Wang YC. Modelling and design method for static resistance of a new connection between steel tubular column and flat concrete slab. J Constr Steel Res 2020;173:106254.
[2] Yu JL, Wang YC. Punching shear behavior of an innovative connection between steel-tubular column and flat-concrete slab. J Struct Eng 2020;146(8):04020159.
[3] Isufi B, Ramos AP. A review of tests on slab-column connections with advanced concrete materials. Structures 2021;32:849–60.
[4] Liu Y, Zhang W, Zhou M, Hou W, Zhang Y. Punching shear performance of star-shaped steel plates reinforced RC slab-column connections. Case Stud Constr Mater 2023;19:e02570.
[5] Hamoda A, Emara M, Mansour W. Behavior of steel I-beam embedded in normal and steel fiber reinforced concrete incorporating demountable bolted connectors. Compos Part B: Eng 2019;174:106996.
[6] Qi J, Cheng Z, Zhou K, Zhu Y, Wang J, Bao Y. Experimental and theoretical investigations of UHPC-NC composite slabs subjected to punching shear-flexural failure. J Build Eng 2021;44:102662.
[7] Kadhim MMA, Saleh AR, Cunningham LS, Semendary AA. Numerical investigation of non-shear-reinforced UHPC hybrid flat slabs subject to punching shear. Eng Struct 2021;241:112444.
[8] Hamoda A, Hossain KMA. Numerical assessment of slab–column connection additionally reinforced with steel and CFRP bars. Arab J Sci Eng 2019;44(10):8181–204.
[9] Mahmood LJ, Rafiq SK, Muhammad MA. Punching shear behavior of reinforced concrete flat slab column connection containing recycled eggshell powder. Structures 2022;46:1016–28.
[10] Ramadan M, Ors DM, Farghal AM, Afifi A, Zaher AH, Ebid AM. Punching shear behavior of HSC & UHPC post tensioned flat slabs – An experimental study. Results Eng 2023;17:100882.

[11] Santos JBd Melo GdS, Fernández Ruiz MPunching. performance of flat slabs with openings accounting for the influence of moment transfer and shear reinforcement. Eng Struct 2024;303:117461.
[12] Zhou L, Huang Y, Chen B. Punching shear behavior of slab–column connections embedded with steel skeletons. Structures 2021;33:2879–92.
[13] Luu BT, Ngo-Huu C, Nguyen-Minh L. Punching shear capacity of unbonded post-tensioned slab - Concrete filled steel tube column joints with innovative connections: experiment and a new prediction model. J Build Eng 2022;59:104974.
[14] Rafiee S, Hosseini A, Marefat MS. Seismic details for exterior connections of post-tensioned flat slabs to steel columns using steel plates, vertical stiffeners and bolts. J Build Eng 2021;36:102140.
[15] Ungermann J, Schmidt P, Classen M, Hegger J. Eccentric punching tests on column bases – new insights into the inner concrete strain development. Eng Struct 2022;262:114273.
[16] Bassurucu M, Turk K, Turgut P. The effect of hybrid fiber and shear stud on the punching performance of flat-slab systems. J Build Eng 2023;77:107555.
[17] Hamoda A, Elsamak G, Emara M, Ahmed M, Liang QQ. Experimental and numerical studies of reinforced concrete beam-to-steel column composite joints subjected to torsional moment. Eng Struct 2023;275:115219.
[18] Hamoda AA, Ahmed M, Abadel AA, Ghalla M, Patel VI, Liang QQ. Experimental and numerical studies of circular precast concrete slender columns with intermediate connection filled with high-performance concrete. Structures 2023;57:105204.
[19] Wang Z, Yan J, Lin Y, Fan F. Influence of shear connectors on the ultimate capacity of steel-UHPC-steel slabs subjected to concentrated loads. Eng Struct 2021;231:111763.
[20] Yehia E, Hussein Khalil A, Mostafa E-E, Abdelfattah El-Nazzer M. Experimental and numerical investigation on punching behavior of ultra-high performance concrete flat slabs. Ain Shams Eng J 2023;14(10):102208.
[21] Cakmak F, Menkulasi F, Dogu M. Punching shear capacity of nonprestressed UHPFRC flat plates: evaluation of existing methods. Eng Struct 2023;280:115662.
[22] El Zareef MA, Abdulrahaman AG, Alnemari A. Experimental investigation of punching shear behaviour of ultra-high performance self-compacting concrete slabs. Case Stud Constr Mater 2023;19:e02307.
[23] Zhou K, Qi J, Wang J. Post-cracking punching shear behavior of concrete flat slabs partially reinforced with full-depth UHPC: Experiment and mechanical model. Eng Struct 2023;275:115313.
[24] Fang Z, Wu J, Xu X, Ma Y, Fang S, Zhao G, et al. Grouped rubber-sleeved studs–UHPC pocket connections in prefabricated steel–UHPC composite beams: shear performance under monotonic and cyclic loadings. Eng Struct 2024;305:117781.
[25] Fang Z, Wu J, Zhao G, Fang S, Ma Y, Jiang H. Shear performance and design recommendations of single embedded nut bolted shear connectors in prefabricated steel–UHPC composite beams. Steel Compos Struct 2024;50:319–36.
[26] Ramos A, Isufi B, Marreiros R, Bolešová M, Gajdošová K. Rational use of HPFRC in slab–column connections under reversed horizontal cyclic loading. Eng Struct 2022;270:114903.
[27] Isufi B, Relvas JP, Marchao C, Ramos AP. Behavior of flat slabs with partial use of high-performance fiber reinforced concrete under monotonic vertical loading. Eng Struct 2022;264:114471.
[28] Yu K-Q, Lu Z-D, Dai J-G, Shah SP. Direct tensile properties and stress–strain model of UHP-ECC. J Mater Civ Eng 2020;32(1):04019334.
[29] Zeng J-J, Pan B-Z, Fan T-H, Zhuge Y, Liu F, Li L-J. Shear behavior of FRP-UHPC tubular beams. Compos Struct 2023;307:116576.
[30] ASTM C39/C39M Standard Test Method for Compressive Strength of Cylindrical Concrete Specimens. American Society for Testing and Materials, USA. 2021.
[31] ACI 318–19-Building Code Requirements for Reinforced Concrete. American Concrete Institute, Farmington Hills, MI, USA. 2019.
[32] ASTM C469/C469M Standard Test Method for Static Modulus of Elasticity and Poisson's Ratio of Concrete in Compression. American Society for Testing and Materials, USA. 2022.
[33] Yu K-Q, Yu J-T, Dai J-G, Lu Z-D, Shah SP. Development of ultra-high performance engineered cementitious composites using polyethylene (PE) fibers. Constr Build Mater 2018;158:217–27.
[34] Mao W-H, Liu J-P, Ding Y. High-modulus and low-shrinkage hybrid-fiber reinforced engineered cementitious composites (ECC). Mater Struct 2022;55(3):87.
[35] ASTM C1583/C1583M-20-Standard Test Method for Tensile Strength of Concrete Surfaces and the Bond Strength or Tensile Strength of Concrete Repair and Overlay Materials by Direct Tension (Pull-off Method). American Society for Testing and Materials, USA. 2020.
[36] Carreira DJ, Chu K-H. Stress-strain relationship for plain concrete in compression. *J Proc* 1985;vol. 82(6):797–804.
[37] Ge W-J, Ashour AF, Ji X, Cai C, Cao D-F. Flexural behavior of ECC-concrete composite beams reinforced with steel bars. Constr Build Mater 2018;159:175–88.
[38] A370–10 Standard Test Methods and Definitions for Mechanical Testing of Steel Products. USA. 2006.
[39] Mansour W, Li W, Ghalla M, Badawi M, El Zareef MA. Improving the punching capacity of two-way RC flat slabs via external strengthening using various configurations of aluminum sheets. Constr Build Mater 2024;420:135611.
[40] Hamoda A, Shahin RI, Ahmed M, Abadel AA, Baktheer A, Yehia SA. Strengthening of reinforced concrete columns incorporating different configurations of stainless-steel plates. Structures 2024;64:106577.
[41] Hibbitt K. and Sorensen I., "ABAQUS Theory Manual, User Manual and Example Manual," ed: Simulia, Providence, RI, USA, 2000.
[42] Elsamak G, Salama MI, Hamoda A. Behavior of precast segmental beams made of high-strength concrete and ultra-high performance fiber concrete connected by shear keys technique. Arab J Sci Eng 2022:1–17.
[43] Feng J, Fang S, Chen M, Fang Z, Liang W. Effect of joint width on shear behaviour of wet joints using reactive powder concrete with confining stress. Eng Struct 2023;293:116566.
[44] Pogorelko VV, Mayer AE. Dynamic tensile fracture of iron: molecular dynamics simulations and micromechanical model based on dislocation plasticity. Int J Plast 2023;167:103678.
[45] Sarkar S, Chakraborty S, Nayak S. Identification of optimum reinforcement detailing using tuned CDP parameters in RC beam under drop-weight impact. Eng Fail Anal 2023;146:107116.
[46] Sümer Y, Aktaş M. Defining parameters for concrete damage plasticity model. Chall J Struct Mech 2015;1(3):149–55.
[47] Hamoda A, Ahmed M, Abadel AA, Gohari S. Experimental and numerical investigations of precast circular reinforced concrete slender columns with intermediate connection. Adv Struct Eng 2023;13694332231222091.
[48] Hamoda A, Ahmed M, Ghalla M, Liang QQ, Abadel AA. Flexural performance of precast circular reinforced concrete members with intermediate connection filled with ultra-high-performance-concrete. Case Stud Constr Mater 2023;19:e02386.
[49] Emara M, Hamoda A, Hu JW. Numerical assessment of rectangular one- and two-way RC slabs strengthened with CFRP under impact loads. Comput Concr 2023;31(3):173–84.
[50] Elsamak G, Salama MI, Hamoda A. Behavior of precast segmental beams made of high-strength concrete and ultra-high performance fiber concrete connected by shear keys technique. Arab J Sci Eng 2023;48(4):4907–23.
[51] Hamoda A, Emara M, Abdelazeem F, Ahmed M. Experimental and numerical analysis of RC beams strengthened with ECC and stainless steel strips. Mag Concr Res 2023;75(5):251–70.
[52] Hamoda A, Ahmed M, Sennah K. Experimental and numerical investigations of the effectiveness of engineered cementitious composites and stainless steel plates in shear strengthening of reinforced concrete beams. Struct Concr 2023;24(2):2778–99.